Uneven flows: On cosmic bulk flows, local observers, and gravity

Wojciech A. Hellwing,[1] Maciej Bilicki,[2,3] and Noam I. Libeskind[4]
[1]Center for Theoretical Physics, Polish Academy of Sciences,
Aleja Lotników 32/46, 02-668 Warsaw, Poland
[2]Leiden Observatory, Leiden University, Niels Bohrweg 2, NL-2333 CA Leiden, The Netherlands
[3]National Centre for Nuclear Research, Astrophysics Division, P.O. Box 447, 90-950 Łódź, Poland
[4]Leibniz-Institut für Astrophysik Potsdam (AIP), An der Sternwarte 16, D-14482 Potsdam, Germany

(Received 20 February 2018; published 18 May 2018)

Using N-body simulations we study the impact of various systematic effects on the low-order moments of the cosmic velocity field: the bulk flow (BF) and the cosmic Mach number (CMN). We consider two types of systematics: those related to survey properties and those induced by the observer's location in the Universe. In the former category we model sparse sampling, velocity errors, and survey incompleteness (radial and geometrical). In the latter, we consider local group (LG) analogue observers, placed in a specific location within the cosmic web, satisfying various observational criteria. We differentiate such LG observers from Copernican ones, who are at random locations. We report strong systematic effects on the measured BF and CMN induced by sparse sampling, velocity errors and radial incompleteness. For BF most of these effects exceed 10% for scales $R \lesssim 100h^{-1}$ Mpc. For CMN some of these systematics can be catastrophically large (i.e., $> 50\%$) also on bigger scales. Moreover, we find that the position of the observer in the cosmic web significantly affects the locally measured BF (CMN), with effects as large as $\sim$20% (30%) at $R \lesssim 50h^{-1}$ Mpc for a LG-like observer as compared to a random one. This effect is comparable to the sample variance at the same scales. Such location-dependent effects have not been considered previously in BF and CMN studies and here we report their magnitude and scale for the first time. To highlight the importance of these systematics, we additionally study a model of modified gravity with $\sim$15% enhanced growth rate (compared to general relativity). We found that the systematic effects can mimic the modified gravity signal. The worst-case scenario is realized for a case of a LG-like observer, when the effects induced by local structures are degenerate with the enhanced growth rate fostered by modified gravity. Our results indicate that dedicated constrained simulations and realistic mock galaxy catalogs will be absolutely necessary to fully benefit from the statistical power of the forthcoming peculiar velocity data from surveys such as TAIPAN, WALLABY, COSMICFLOWS-4 and SKA.

DOI: 10.1103/PhysRevD.97.103519

I. INTRODUCTION

The standard model of cosmology—Lambda cold dark matter (LCDM)—is extremely successful in explaining a plethora of observations. These include the features of the cosmic microwave background, i.e., [1,2], the primordial nucleosynthesis and light element abundances [3,4], the growth of primordial density perturbations into the present-day large-scale structure (LSS) [5–7], as well as the late-time accelerated expansion of the Universe [8–11]. However, since LCDM is mostly phenomenological in its nature, this spectacular success comes at a price of accepting that the main contributors to the cosmic energy budget are dark matter (DM) and dark energy (DE), which have not been directly detected in any experiments so far. Therefore, it is desirable to look for other probes of the cosmological model, especially those which do not share at least some of the systematics of the aforementioned measurements.

In this context, the peculiar motions of galaxies—i.e., deviations from the uniform Hubble flow—are considered as particularly valuable [12–14]. Induced by gravity only, they are not affected by such systematics as galaxy bias, which plagues for instance the measurements of galaxy clustering. Peculiar velocities can be therefore used, at least in principle, to obtain constraints on various cosmological parameters such as the mean matter density or the growth of structure [15,16], independently of other methods.

Arguably the most popular statistic of the velocity field is the bulk flow (BF), i.e., the net peculiar motion of galaxies contained in a given volume. BF probes large-scale fluctuations of matter distribution, and should generally diminish with increased volume. Over the decades, BF measurements have often been subject to various controversies. An example from early studies is by [17], who measured a net motion of Abell clusters amounting to $\sim$700 km s^{-1} within a radius of 15,000 km s^{-1}, which was

however not confirmed by subsequent analyses, e.g., [18,19] (but see [20]). More recently, the authos of [21] claimed significant BF ($\sim 400\ \mathrm{km\,s^{-1}}$) on scales of $\sim 100h^{-1}$ Mpc from a combined sample of galaxies and clusters, which also is not supported by several other studies, e.g., [15,22] (see however [23]). Even more controversial are the claims of the very large scale ($\sim 300h^{-1}$ Mpc) "dark flow" by [24], which again is not corroborated by related analyses [25,26]. Thanks to the ever growing amount of observational data, there is continued interest in measuring the BF and, if these discrepancies could be resolved, using it as a cosmological probe; for some more recent results see [27–43].

Part of the BF "controversy" (or more precisely, inconsistency between some measurements) is due to the fact that many of the BF assessments are not directly comparable due to different estimators used, with specific sensitivity to various scales and systematics [44–46]. The quality and volume of the velocity data is another important issue here. We note that some of the developed estimators do not use peculiar velocities at all to estimate the BF, e.g., [24,28,30,31,34,37], they are thus not sensitive to the related biases, although this of course does not make them immune to other, often major, systematic effects.

The BF continues to be regarded as a promising probe of cosmology especially taking into account that larger, denser, and more accurate samples of peculiar velocities are expected to appear in the coming years from such surveys as Taipan [47], WALLABY [48], or COSMICFLOWS-4 [49]. However, agreement is gradually building up that in order to take full advantage of these future data sets for BF and other velocity-based measurements, the control of systematic effects and biases is crucial for proper data interpretation. Recent developments of e.g., [45,50,51] highlight the importance of selection and observer-driven effects for peculiar velocity studies. Reference [45] considered the impact of purely geometrical selection effects on the inferred bulk flows, including the partial sky coverage. In addition, Ref. [51] investigated mainly the effect of different radial selection functions and the corresponding galaxy/halo weighting. Both works report the importance of these two systematic effects that can bias the data, but the effect they studied referred to a hypothetical Copernican observer. The results of [50] however underline that for relatively shallow and sparse velocity data, the specific location of the observer within the cosmic web affects in a nontrivial way the cosmic variance of the velocity observables. Inspired by these previous results, in this work we will readdress this issue by looking closely at the impact of the observer location (i.e., importance of the local cosmic structures) on the inferred BF and related statistics. We will show that the BF itself is very sensitive to such effects, which must be therefore properly accounted for when measuring it from the current and forthcoming data sets.

A statistics related to the BF, which uses additionally the third moment of the peculiar velocity field, is the cosmic Mach number (CMN) defined as the ratio of the BF to the peculiar velocity dispersion in the same volume [52]. In the original proposal, CMN was regarded as a "critical test for current theories," and more recently quoted as "a sensitive probe for the growth of structure" [53]. For other theoretical and observational studies of CMN and its importance for cosmology, see [54–58]. In this paper we will examine the sensitivity of the CMN to the same systematics as those studies for the BF. Similar conclusions regarding the importance of such effects for CMN as in the case of BF will apply.

The cosmic velocity field reflects a continuous action of gravity integrated over the history of large-scale-structure growth. Thus it offers, in principle, a very sensitive probe of the very nature of gravity itself. Here, even small possible deviations from a general relativity (GR)-like force law provide minute galaxy acceleration changes that are amplified when integrated over time. This has been shown by other authors for a range of velocity field statistics and viable modified gravity (MG) models (see e.g., [59–61]). Thus, if one is able to control various systematic effects, and in the case of known (assumed) cosmological parameters like Ω_m and σ_8 (taken for example from CMB observations), then the galaxy velocity field (and its low-order moments) provides a potentially powerful way of constraining non-GR models. Such constraints would foster an independent, thus complementary, way of testing GR and measuring the local value of the growth rate, $f \equiv \ln D_+ / \ln a$ [13,14]. In order to be able to use the velocity data for testing gravity one needs to recognize and control all important systematic effects. Consequently, in this paper we also consider a modified gravity model (deviating by $\sim 15\%$ in the growth rate from GR) and compare its signal with the magnitude of various systematics in the GR case.

As briefly indicated above, various systematic and statistical effects that disturb the velocity data were a subject of careful study in the past. However, except for the early work of Ref. [62], analyses of the impact of a specific location of the observer within the large-scale structure were not conducted. Reference [62] studied only the two-point velocity statistics and they did not require the presence of any nearby cosmic web structures such as the Virgo cluster. Here, we will conduct a joint study of various systematic effects, starting from sparse sampling and radial selection, up to the impact of the observer location. We will identify scales and magnitudes of various effects and compare them against expected statistical fluctuations in a systematic fashion. In this way we will obtain insight into scales, magnitudes and the interdependence of various systematical effects troubling BF and CMN measurements. This will constitute another important step for peculiar velocity studies towards the precision cosmology era.

The paper is organized as follows: in Sec. II we describe in detail computer simulations used in this study; in Sec. III some theoretical preliminaries and relevant considerations are given; Sec. IV contains a description of mock catalogs and various observational effects that we model; in Sec. V we discuss the effects induced by systematics independent from a specific observer's position, while in Sec. VI the focus is given to signals measured by local group-analogue observers; Sec. VII compares signal from a modified gravity model with known GR systematic effects. Finally Sec. VIII summarizes our findings; this is followed by Sec. IX where discussion and conclusions are given. Some additional tests and discussion about the influence of the simulation box size are given in the Appendix.

II. SIMULATIONS

To study cosmic flows we employ a set of large N-body simulations conducted with the use of the ECOSMOG code [63]. Time evolution of cosmic structures is here followed with respect to a background spatially flat Universe described by cosmological parameters consistent with the 2013 results from the Planck mission [64]. We imposed the following values: $\sigma_8 = 0.831$, $\Omega_m = 0.315$, $\Omega_\Lambda = 0.684$, $n_s = 0.96$. The growth of density fluctuations is modeled by assuming that all nonrelativistic matter is collisionless, i.e., we treat the baryonic component as DM. Ignoring baryonic physics will not introduce any significant biases as long as we are not interested in internal properties of individual halos but only in their spatial distribution and peculiar velocities (e.g., [65]). Thus in our simulation we place 1400^3 DM particles in a cubic box of comoving size of $1000h^{-1}$ Mpc. This particular setup fixes the mass resolution at $m_p = 3.2 \times 10^{10} h^{-1}\ M_\odot$. ECOSMOG is an extension of the RAMSES code [66] and uses adaptive mesh refinement (AMR) and dynamical grid relaxation methods to compute the gravitational potential and forces. Thus our simulations are not characterized by a single fixed force resolution, but to gauge our dynamical spatial resolution we can use the cell size of the most refined AMR grid. In all our runs such a grid had a rank of $N17$ resulting in the finest force resolution of $\varepsilon = 7.6h^{-1}$ kpc. However, the average force resolution was around $35h^{-1}$ kpc.

In this paper we aim to study various systematic effects that affect the lowest moments of the cosmic velocity field. For that reason we will be mostly concerned with the fiducial cosmological ΛCDM model. However, in Sec. VII we will compare the magnitude of various systematics with the predicted amplitude of a non-GR signature expected in the case of a modified gravity model. As a representative guinea pig we chose the so-called normal branch of the Dvali-Gabadadze-Poratti (henceforth nDGP) model [67,68]. For a more detailed description of that model and its implementation in simulations, see the relevant section.

Real astronomical observations measure the radial component of the peculiar velocity of a galaxy rather than of its host halo. Our simulations do not attempt to model assembly of galaxies in any way, but we can safely use the bulk velocities of DM halos found in our simulations as faithful proxies for real galaxy peculiar velocities. This is the case since the studies of other authors, e.g., [65,69], have shown that for central galaxies residing in massive halos their relative velocities with respect to their host halos are very small (i.e., $\lesssim 5$ km s^{-1}) compared to the bulk-flow magnitude we will study here. In addition we do not expect that any nonzero galaxy velocity in relation to its host halo would be correlated to the large-scale matter distribution which induces bulk flows. Thus, due to global isotropy these velocities should average out to zero for scales much larger than a given halo radius.

To identify halos and subhalos in the simulations we employ ROCKSTAR [70], a phase-space friends-of-friends halo finder. To define a halo edge we use the virial radius R_{200}, defined as the radius within which the enclosed density is $200 \times \rho_c$, where ρ_c is the critical cosmic density. For further analysis we keep all gravitationally bound halos that contain at least 20 DM particles each. This sets our minimal halo mass to $M_{\rm min} = 20 \times m_p = 6.4 \times 10^{11} h^{-1}\ M_\odot$. Based on the initial halo catalogs, we build our test halo populations by distinguishing the central halos from satellites (subhalos). For further analysis we keep only the centrals, which we will treat as rough mocks for population of central galaxies. To obtain additional halo samples with lower number densities we perform random subsampling. Our main catalog includes all central halos resolved in our simulation at $z = 0$ and has a number density of $\langle n \rangle = 6 \times 10^{-3} h^3$ Mpc^{-3}. To obtain sparser samples we consequently dilute this main sample by randomly (and spatially uniformly) keeping only every nth halo. Thus we also obtain the following samples: $\langle n \rangle = 5 \times 10^{-4} h^3$ Mpc^{-3}, $\langle n \rangle = 5 \times 10^{-5} h^3$ Mpc^{-3} and $\langle n \rangle = 5 \times 10^{-6} h^3$ Mpc^{-3}. Such number densities of tracers are in the range one can encounter in current and future astronomical observations: from complete rich local universe surveys (see e.g., [47,71,72]), through Luminous Red Galaxy samples from redshift surveys (e.g., [73,74]), to quasar and Supernova data (e.g., [75,76]).

Finally, since peculiar velocity catalogs are rather shallow, rarely reaching at present deeper than $\sim 200h^{-1}$ Mpc (see e.g., [43,49,77,78]) we constrain all our analysis only to the $z = 0$ snapshot of our simulations and to scales up to $250h^{-1}$ Mpc. This being said, it is also imperative to comment on the convergence of the simulation results at large scales. The velocity field is much more sensitive to contributions from perturbation modes much larger than a given scale one considers. In other words, we can expect that the finite-volume effects will be more pronounced here than in the case of the density field. To check what scales we can trust, we have run additional tests involving three more simplified simulations with a varying box size. The details and analysis of these are given in the Appendix. The results of these tests indicate that on scales $R \gtrsim 200h^{-1}$ Mpc the

amplitude of our BF is systematically biased down by 15% or more. However, the size of various systematic effects expressed as a relative BF magnitude difference appears to be only weakly affected by the box size up to $R \sim 250h^{-1}$ Mpc. This supports our choice of the maximal scale we consider in this paper.

III. THEORETICAL PRELIMINARIES

Throughout our work we assume the homogeneous and isotropic cosmological model, in which the background obeys Friedman-Lemâitre equations with a scale factor $a(t)$. All the quantities will be expressed in comoving coordinates, i.e., $\vec{x} = \vec{r}/a(t)$. For background density $\rho_b(t)$ and density contrast $\delta(\vec{x},t) \equiv \rho(\vec{x},t)/\rho_b(t) - 1$, the Poisson equation linking the peculiar gravitational potential $\phi(\vec{x},t)$ with density perturbations is

$$\nabla^2\phi(\vec{x},t) = 4\pi G\rho_b(t)a^2\delta(\vec{x},t). \tag{1}$$

By integration, we obtain the expression for peculiar accelerations $\vec{g}$ [79]:

$$\vec{g}(\vec{x}) = -\frac{\nabla\phi}{a} = Ga\rho_0 \int \frac{\delta(\vec{x'})(\vec{x'}-\vec{x})}{|\vec{x'}-\vec{x}|^3}\mathrm{d}\vec{x'}. \tag{2}$$

Peculiar velocities $\vec{v}(\vec{x},t)$, defined as deviations from the Hubble flow, are coupled to the density field via the continuity equation:

$$\frac{\partial\delta}{\partial t} + \frac{1}{a}\nabla\cdot[(1+\delta)\vec{v}] = 0. \tag{3}$$

A. Linear theory predictions

We can model the cosmic velocity field by performing a decomposition of the full three-dimensional (3D) field into a sum of longitudinal (nonrotational) and transverse (rotational) components:

$$\vec{v} = \vec{v_L} + \vec{v_T}, \quad \text{where:} \tag{4}$$

$$\nabla\times\vec{v_L} = 0 \quad \text{and} \quad \nabla\cdot\vec{v_T} = 0. \tag{5}$$

In the linear regime, the velocity field is curl-free, thus $\vec{v_T} = 0$ and the field is purely potential. Henceforth it can be expressed as a gradient of a scalar function Ψ_v (called the velocity potential):

$$\vec{v} = -\nabla\Psi_v/a. \tag{6}$$

Now considering the continuity equation (3) it can be shown that the velocity potential obeys

$$\nabla^2\Psi_v = Hfa^2\delta, \tag{7}$$

where we have used the definition of the dimensionless growth rate $f \equiv \mathrm{d}\log D_1/\mathrm{d}\log a$. The growth rate only very weakly depends on Λ [80] and for a flat LCDM universe $f \approx \Omega_m^{0.55}$ [81]. However, in general for some alternative cosmologies (like coupled DE or modified gravity) it can take a different value and also be a scale-dependent function.

Finally, in the linear regime we have $\phi \propto \Psi_v$ and $\vec{v} \propto \vec{g}$ (where $\vec{g}$ is the peculiar gravitational acceleration), and in particular at $z = 0$ one has

$$\vec{v} = \frac{H_0 f}{4\pi G\rho_0}\vec{g} = \frac{2f}{3H_0\Omega_m}\vec{g}. \tag{8}$$

In the linear regime we can also express the relation between the power spectrum of density fluctuations, $P(k) \equiv \langle\delta_k\delta_k^*\rangle$, and the dimensionless expansion scalar, θ_k, which is the scaled velocity divergence (also called the expansion scalar)

$$\theta \equiv \frac{-\nabla\vec{v}}{aH_0}, \text{ and } \vec{v}_k = aH_0\frac{i\vec{k}}{k^2}\theta_k, \quad \text{so} P_{\theta\theta}(k) = \langle\theta_k\theta_k^*\rangle. \tag{9}$$

In the linear regime for a potential flow it follows from the continuity equation (3) that

$$P(k) = f^{-2}P_{\theta\theta}(k). \tag{10}$$

The above relation is often used in the literature to approximate velocity power spectrum by linear velocity divergence, thus neglecting dispersion and vorticity (see e.g., [12]). Such approximation however holds only on sufficiently large scales; those scales are generally larger (i.e., ≥ 60–$100h^{-1}$ Mpc) than in relevant analyses of the density field (see e.g., [82–84]).

B. Bulk flow, velocity dispersion, and cosmic Mach number

The bulk flow (BF) is the dipole (second) moment of the peculiar velocity field, $\vec{v}(\vec{x})$, in a given region of space (volume). Nonzero BF reflects a net streaming motion towards a particular direction in space. Thus in the continuous limit of the field $\vec{v}$, for a spherical region with a radius R, it will be

$$\vec{\mathcal{B}}(R) = \frac{3}{4\pi R^3}\int_0^R \vec{v}(\vec{x})\mathrm{d}^3x. \tag{11}$$

Throughout this paper we will interchangeably use BF and $\mathcal{B}$ to denote the bulk flow amplitude.

When the velocity field is sampled by a set of N discrete tracers (e.g., galaxies) then the above integral becomes a finite sum. If each individual galaxy is assigned a weight w_i, then the 3D bulk flow vector will be

$$\vec{\mathcal{B}}(R) = \frac{\sum_{i=1}^N w_i\vec{v}_i}{\sum_{i=1}^N w_i}, \tag{12}$$

where $\vec{v}_i$ is the peculiar velocity of the ith galaxy. An important note to make here is that since galaxies are biased tracers, they do not sample the underlying smooth density and velocity fields evenly. Since they are preferentially found in high-density regions, galaxies by construction give mass-weighted fields. This is in contrast to Eq. (11), which is defined for a volume-weighted velocity field. In the linear regime (or in the limit of bias $b \to 1$) the two definitions should agree. On small, nonlinear scales, we can expect that discrete tracer-based estimators, such as Eq. (12), will be biased. We should remember about this whenever we compare linear theory predictions with the estimators based on discrete tracers such as galaxies. If the density fluctuations are a random Gaussian field, then in the linear theory (i.e., on sufficiently large scales) the corresponding velocity field will also be a random variable (for each vector component separately and independently) with a zero mean. Then we can define the corresponding dispersion (VD) of the peculiar velocities with respect to the averaged bulk flow as

$$\mathcal{D}(R) = \frac{\sum_{i=1}^{N} [w_i \vec{v}_i - \vec{\mathcal{B}}(R)]^2}{\sum_{i=1}^{N} w_i - 1}, \tag{13}$$

where the sum of the weights needs to be $\neq 1$, so the denominator does not take a zero value. The variance of the velocity field will be given by the velocity power spectrum $(2\pi)^3 \delta^D(\vec{k} - \vec{k'}) P_{vv}(k) \equiv \langle v_{\vec{k}}^2 \rangle$, where $v_k = |\vec{v}_{\vec{k}}|$ and we already assumed global isotropy ($k = |\vec{k}|$). Thus the predicted root mean square value of the bulk flow amplitude is

$$\mathcal{B}^2(R) = \frac{1}{2\pi^2} \int \mathrm{d}k k^2 P_{vv}(k) |\hat{W}(kR)|^2. \tag{14}$$

Here $\hat{W}(kR)$ is the Fourier image of the window function. Usually one takes W to be spherical top-hat, which implies $\hat{W}_{TH}(kR) = 3[\sin(kR) - kR\cos(kR)]/(kR)^3$, but some authors consider also the so-called all-sky Gaussian selection function with $\hat{W}_G = \exp(-k^2R^2/2)$.

Now, if there is no velocity bias and the velocity field is curl-free, then $P_{vv}(k) = k^{-2} H_0^2 P_{\theta\theta}(k)$, and Eq. (14) becomes

$$\mathcal{B}^2(R) = \frac{H_0^2}{2\pi^2} \int \mathrm{d}k P_{\theta\theta}(k) |\hat{W}(kR)|^2. \tag{15}$$

In the regime where the velocity vorticity is negligible and Eq. (10) holds, one finally obtains

$$\mathcal{B}^2(R) = \frac{H_0^2 f^2}{2\pi^2} \int \mathrm{d}k P(k) |\hat{W}(kR)|^2. \tag{16}$$

The above equation is commonly used as the linear theory prediction for the bulk-flow amplitude in a universe described by a particular choice of $P(k)$ and f. Consequently, the corresponding variance of the residual velocity field (after the BF was subtracted) for that case takes the form

$$\mathcal{D}^2(R) = \frac{H_0^2 f^2}{2\pi^2} \int \mathrm{d}k P(k) (1 - |\hat{W}(kR)|^2). \tag{17}$$

Now to obtain predictions for the bulk flow amplitude and some significance intervals, a model distribution function for peculiar velocities is needed. This is obtained by noticing that for sufficiently large smoothing scales, the distribution for a single velocity component approaches a Gaussian, thus the distribution for the bulk flow magnitude becomes Maxwellian (see [85,86]). Hence for a velocity field $\vec{v}(R)$ with rms velocity of $\mathcal{B}$, this is given by

$$p(v)\mathrm{d}v = \sqrt{\frac{2}{\pi}} \left(\frac{3}{\mathcal{B}^2}\right)^{3/2} v^2 \exp\left(-\frac{3v^2}{2\mathcal{B}^2}\right) \mathrm{d}v. \tag{18}$$

Considering $\mathrm{d}p(v)/\mathrm{d}v = 0$ gives in the limit the most likely value (MLV) $\mathcal{B}_{MLV} = \sqrt{2/3}\mathcal{B}$ and the expected value (EV) $\langle v \rangle = \mathcal{B}_{EV} = 2\mathcal{B}_{MLV}/\sqrt{\pi} = \sqrt{8/3\pi}\mathcal{B}$. MLV and EV are widely used as common linear theory (LT) predictions for the BF amplitude, and in the reminder of this manuscript we shall adopt the same strategy whenever we will be invoking LT formulas. We caution however, that in this context it is important to bear in mind that such predictions only hold if the distribution of the components of $\vec{v}$ are Gaussian. The validity of this assumption depends on scales which one considers. Although in general it was established that for most scales dealt with in modern velocity analysis (i.e., $\gtrsim 30h^{-1}$ Mpc) this assumption generally holds [45], results shown by other authors imply that caution should be taken (see also [82,83]).

A separate note should be made here about the limits of the integrals used to calculate $\mathcal{B}(R)$ and $\mathcal{D}(R)$ from Eqs. (14)–(17). To obtain predictions for the physical Universe one should consider the obvious limits from $k_{\min} = 0$ to $k_{\max} = \infty$. However, when we want to compare LT predictions with numerical simulations that used some finite computation box, we should account for the fact that the modeled velocity field will miss the contribution from the modes larger than the box length L. Also due to discretization of both mass and volume there is some characteristic minimal scale that is still resolved by the simulation, usually taken to be the force resolution ε. In such a case, the corresponding integration limits are then $\frac{2\pi}{L} \leq k \leq \frac{2\pi}{\varepsilon}$. Whenever we will be comparing LT predictions with the simulation results we will employ the above integration limits.

Some authors [52,53,58] advocated also another type of statistics, namely the cosmic Mach number (CMN, or $\mathcal{M}$), that we can define now as

$$\mathcal{M}(R) \equiv \frac{\mathcal{B}(R)}{\mathcal{D}(R)}, \tag{19}$$

which in the linear regime should be only a function of the shape of the matter power spectrum [or the effective slope of $\sigma^2(R)$ around $\sim R$] [54,55,87].

The above considerations suggest that the linear theory prediction for the bulk flow and associated statistics should strongly depend on two parameters of the underlying cosmological model, namely the growth rate f and the amplitude of $P(k)$, which can be evaluated by the σ_8 parameter. These dependencies have motivated many authors to advocate the use of the low-order velocity field statistics as cosmological probes [12–14,22,28,30,37,38,42,53].

To gauge the magnitude of variations and their co-dependence on f and σ_8 we have considered a number of power spectra variants. The fiducial case is (i) the Planck13 cosmology ([64]; the same as used in our simulations) and we also examined four cases: (ii) high Ω_m ($\Omega_m = 0.35, \Omega_\Lambda = 0.65$); (iii) low Ω_m ($\Omega_m = 0.25, \Omega_\Lambda = 0.75$); (iv) high σ_8 ($= 0.9$) and (v) low σ_8 ($= 0.75$). Here, for each case (i)–(v) we kept fixed all the remaining ΛCDM parameters, imposing $\Omega_k = 0$ and $\Omega_{\rm tot} = 1$, and varied only the value of a given matter density or power spectrum normalization. By changing Ω_m we probe different values of the growth rate (by $\sim 10\%$ around the fiducial case) and by varying σ_8 we sample different power spectrum amplitudes. For all the cases we have used the CAMB software package [88] to obtain high-accuracy linear matter power spectra and then applied the HALOFIT model [89] to evolve the spectra to the nonlinear regime. In addition, we also considered one more case, where we used the fully nonlinear $P_{\theta\theta}$ estimated from our ΛCDM simulation. The nonlinear velocity divergence power spectrum was used only for $k > 0.01h$ Mpc^{-1}, where it deviates by more than 3% from the nonlinear $f^2P(k)$; for smaller k it was substituted by the CAMB-provided $P(k)$, rescaled by f^2. We checked the effect of the nonlinear divergence spectra, since the scales at which the velocity field is curl-free and the scales at which $\delta \ll 1$ are not necessary the same [83,84].

In Fig. 1 we compare all the examined power spectra with our fiducial Planck13 case (i). The velocity divergence power spectrum was scaled by the corresponding f^2 factor. We can observe that for the cases where Ω_m is varied, the corresponding changes in $P(k)$ are limited to large scales, $k \leq 0.1h$ Mpc^{-1}. Small deviations seen above $k \gtrsim 3h$ Mpc^{-1} reflect the different length of the matter-dominated epochs in low and high-Ω_m universes and so different degree of nonlinearity in the density field. However, this appears at scales too small to be relevant for the large-scale velocity field. As expected the high-(low-)Ω_m case is characterized by a smaller (larger) amplitude of the power spectrum than the fiducial case at these scales. For both cases the changes in the large-scale $P(k)$ amplitudes are quite dramatic. Variations in σ_8 alone affect the spectrum on all scales, but the overall effect is much smaller (typically within $< 25\%$). Here we can also

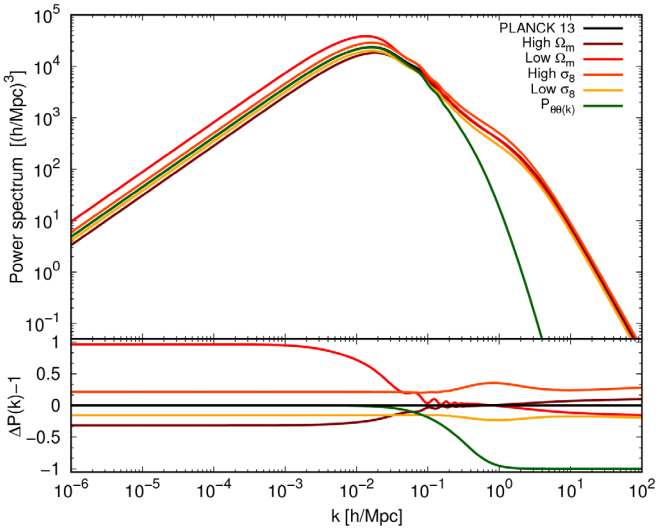

FIG. 1. Comparison of the nonlinear Planck13 cosmology power spectrum (black solid line) with its variants computed for high and low values of Ω_m and σ_8 parameters. In addition, the corresponding nonlinear velocity $P_{\theta\theta}(k)$ is also plotted with a short-dash-dotted green line. The upper panel shows the absolute values, while the bottom panel presents the relative difference with respect to the Planck13 case.

note that the small-scale variance of $P_{\theta\theta}(k)$ is strongly suppressed compared to the matter $P(k)$. This is expected, once one considers that in the nonlinear regime, while the collapsed objects increase the density field variance, the corresponding velocity field around and inside those objects attains a high degree of vorticity and dispersion due to shell crossing and virialization [84,90–92].

Figure 2 illustrates the changes, imposed due to variations in $P(k)$ shape and amplitude, in the corresponding

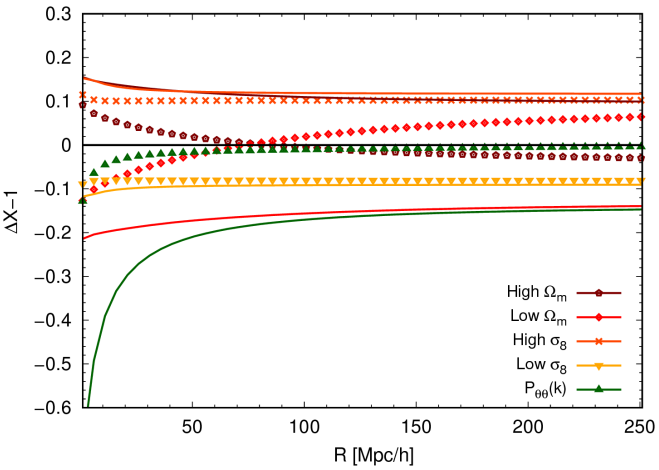

FIG. 2. The relative difference of linear theory predictions for the bulk flow magnitude $\mathcal{B}(R)$ and the velocity dispersion $\mathcal{D}(R)$ as predicted by equations (15)–(17) taken with respect to the fiducial case where Planck13 nonlinear matter power spectrum was used. The symbols mark the results for the bulk flow amplitudes, while the matching color lines are for the corresponding velocity dispersion.

estimated $\mathcal{B}$ (symbols) and $\mathcal{D}$ (lines). The previously seen dramatic differences in $P(k)$ amplitudes are translated to rather mild impact on the resulting linear-theory bulk flows. Here, for most cases, the changes are within $\sim 10\%$, thus of the same magnitude as our variations in both f and σ_8. We can also notice the known $\Omega_m - \sigma_8$ degeneracy, where the effect of increasing one parameter can be to a large extent compensated by the decrease of the other. The effect of using the nonlinear $P_{\theta\theta}(k)$ to predict $\mathcal{B}$ is minimal for $R > 50h^{-1}$ Mpc. In contrast, the use of the nonlinear velocity divergence power spectrum results in a much more dramatic effect onto the $\mathcal{D}$ estimator. This suggests that modeling of nonlinearities in the density and velocity field is not that important for $\mathcal{B}$ predictors, but might be crucial for the prediction of the expected Mach number. The latter fact was already emphasized to some extent by [58], who noticed that in order to obtain more accurate predictions for the Mach number some nonlinear corrections for $\mathcal{D}$ have to be applied. This reflects the fact that the velocity dispersion is intrinsically a local quantity, and nonlinear effects such as virialization and shell crossing have a significant effect (see e.g., [93–95]).

IV. THE VELOCITY MOCKS AND NONLINEAR OBSERVABLES

To move beyond the linear theory we employ the set of N-body simulations described in Sec. II. To study various systematics, nonlinear effects and biases, and to get a closer connection with real astronomical observations, we construct a set of mock catalogs and observables from our simulations. As an input for all our analysis we consider halo and subhalo catalogs saved at $z = 0$.

Generally, when considering various observational errors and systematics (like survey geometry, selection function, radial distribution, etc.) one can apply their modeling to the simulation data and then analyze the mock catalog by computing various statistics from it. We adopt this routine approach by calculating various data point weights, which characterize different modeled effects in separate mock catalogs.

We consider the following "observational effects" on the data:

(i) *Observer location.*—All the relevant quantities, such as distances and angles, depend on a specific observer location, whether it would be a random or preselected observer; computations are done in the CMB rest frame.

(ii) *Radial selection.*—We model the following radial selections: *FC*—full completeness (i.e., no radial selection nor distance limit); *CF3*—COSMICFLOWS-3-like [49] selection functions (see below).

(iii) *Geometry/zone of avoidance.*—Since all our catalogs are observer dependent, it is natural to also include the effect of the so-called zone of avoidance (ZoA) caused by obscuration of the far-away objects by the Galactic disk. This is done by removing galaxies from the appropriate part of the volume. See more details below. In our analysis we do not model the importance of particular structures hidden behind the ZoA, such as the Norma Cluster [96] or recently discovered Vela Supercluster [97], as this would require detailed constrained simulations. We postpone such studies for future work.

(iv) *Radial velocity error.*—To model peculiar velocity errors associated with the uncertainties of galaxy scaling relations that are used to infer galaxy velocities from redshifts (see more below).

In our analysis we are concerned with lower-order velocity statistics that are estimated from specific observer-dependent mock catalogs. Therefore, all our results (unless clearly emphasized otherwise) are computed as ensemble averages over all mock observers in a given sample. References [45,51] have shown that the distribution of bulk flows amplitudes inferred from simulations deviates from a Gaussian. We have checked that this is the case for all our samples, both for the bulk flows as well as for the velocity dispersions. For that reason, a simple averaged mean and associated variance might not be a faithful characterization of the underlying ensemble. Thus we decided to use *medians* and associated 16th and 84th percentiles to characterize all our results.

Observer location.—All the observables we discuss later in the paper were estimated for a fixed given number of observer locations. By construction, all our observers must sit in a DM halo. We consider two types of observer locations: random and preselected. Random observers are chosen randomly from all halo positions in a given catalog, while the preselected are contained in a closed list of locations predefined by some user provided criteria. In this paper we consider various criteria of a hypothetical local group (LG)-like observer. See more in Sec. VI.

Radial selection.—Generally, to obtain the desired radial selection, we would have to select multiple times from an input data set according to probability that is proportional to the defined shape of the selection function, keeping finally the data product with mock radial selection that is closest to the imposed one. Such a procedure for large samples as ours is however very unpractical. We decided to use a simple data weighting scheme instead, where each galaxy is given a weight exactly as defined by the input selection function. For a large number of galaxies, the results of both procedures give comparable results. Therefore, since we do not compare our results to any particular galaxy survey, but rather aim at providing general observational data modeling, we are satisfied with the much faster data weighting method. We opt to use the weighting scheme that follows the radial selection of the COSMICFLOWS-3 catalog for the sake of simplicity and generality. CF3 is currently the largest peculiar velocity catalog, thus by studying CF3-like radial selection our

model will be close to the best-case data scenario. In the case *FC* listed above, all the halos have equal unit weights, as in Eq. (12). When modeling the CF3-like radial selection (2), we impose [50]

$$w_h = \begin{cases} 1, & \text{if } r \le r_w \\ (r/r_w)^{-m}, & \text{otherwise.} \end{cases} \tag{20}$$

Here, r_w is the characteristic radial depth of the catalog (in h^{-1} Mpc). For our CF3-like catalogs we consider $r_w = 80h^{-1}$ Mpc and two values for the exponent $m = 2, 3$:

Geometry/zone of avoidance.—Most extragalactic observations, including those of peculiar velocities, do not have access to low Galactic latitudes due to the obscuration by dust, gas, and stars in the Milky Way—the "Zone of Avoidance." To model it, we consider a small opening angle $\alpha_{\rm ZoA} = 10.5$ deg [98] chosen with respect to a fixed observer-dependent local $(x, y, z) = (x_{\rm Obs}, 0, 0)$ plane. Galaxies falling inside $-\alpha_{\rm ZoA} \le \alpha \le \alpha_{\rm ZoA}$ are removed.

Radial velocity error.—Galaxy peculiar velocity surveys rely on redshift-independent distance-indicator relations (DIs) to extract the cosmological and peculiar components from a galaxy redshift. The most commonly used methods are based on galaxy scaling relations, such as Tully-Fisher [99] or fundamental plane [100]. Such methods are unavoidably plagued with significant relative errors on estimated velocities stemming from intrinsic scatter in used relations and various systematic (usually nonlinear) biases. The peculiar velocity errors are a source of a serious worry and their magnitude sets a fundamental limit on cosmic velocity data usability. A constant relative error in distance determination translates here to a velocity uncertainty that grows linearly with galaxy redshift. We attempt to model this by a simple relation of the form

$$\sigma_v = \Delta_v H_0 D_z. \tag{21}$$

Here H_0 is the Hubble parameter, D_z is the galaxy comoving distance and Δ_v models the typical scatter of the logarithmic distance ratio $\eta \equiv \log_{10}(D_z/D_r)$ error. The ratio η is used to estimate the peculiar velocity. Here D_r is the comoving distance to a galaxy inferred via DIs (see more in e.g., [42,49,101]) and the spectroscopic galaxy redshift z. We choose $\Delta_v = 0.25$, which is a conservative value when compared with smaller scatter typically found in modern velocity data [49]. We assume that the above velocity error is Gaussian with zero mean and dispersion σ_v. In reality such an assumption is often broken for various velocity estimators, but we adopt it for simplicity, as non-Gaussian contributions to velocity errors depend strongly on particular galaxy catalog specifics.

Once parameters for mock galaxy catalogs are chosen, we compute the bulk flow and the dispersion of the residual velocity field by assigning specific halo/galaxy weights and using Eqs. (12) and (13). We sum separately over the three Cartesian velocity vector components in concentric spheres of radius R around a fixed observer location. This procedure yields us specific weighted bulk flow components, i.e., $B_x(R)$, $B_y(R)$ and $B_z(R)$. The bulk flow amplitude is then

$$\tilde{B}(R) = \left(\sum_{i=1}^{3} B_i(R)^2\right)^{1/2}. \tag{22}$$

Here the sum runs over three Cartesian components of a 3D velocity vector field and the procedure for the residual velocity dispersion is analogous.

In reality, the above procedure cannot be applied to real data, since except for a very few cases, we do not have full 3D peculiar velocity information. What is directly accessible is only the line-of-sight (LOS) velocity component. Thus for observational data one usually adopts an estimator of the BF that is based on the radial velocity component. For example, in the most popular maximum likelihood (ML) method, the BF components are obtained via

$$\tilde{B}_i = \sum_{n}^{N} w_{i,n} V_n, \tag{23}$$

where i again indicates one of the three Cartesian indexes, V_n is an nth LOS velocity measurement. Here, $w_{i,n}$ is an associated weight of a given velocity measurement, which usually is taken to be

$$w_{i,n} = \sum_{j}^{3} A^{-1}_{ij} \frac{\hat{r}_{n,j}}{\sigma_n^2 + \sigma_*^2}, \tag{24}$$

where $\hat{r}_{n,j}$ is a unit vector from the observer to a given galaxy n, σ_n is the uncertainty of a given velocity measurement, and σ_* describes 1D velocity dispersion due local nonlinear virial motions. The matrix A_{ij} describes geometric moments of the whole sample of tracers, and is given by

$$A_{ij} = \sum_{n}^{N} \frac{\hat{r}_{n,i}\hat{r}_{n,j}}{\sigma_n^2 + \sigma_*^2}. \tag{25}$$

The above estimator is based on the inverse variance weighting method of Ref. [102].

We do not choose to implement the above estimator for various reasons. First, it is uniquely defined for a given astronomical data set, with its specific radial and geometrical selections and errors of velocity estimates. To keep our discussion as general as possible we opt to use a much simpler estimator of Eq. (22) instead. This is justified since the averages over all observers for our mock catalogs will be in practice close to isotropic and spatially uniform. For such a case the geometric matrix A_{ij} is uniform and approximates a product of a constant factor and a unit matrix. In addition, since we only use central halos, contributions from any nonlinear virial motions are strongly suppressed. The last statement does not hold for nonrelaxed systems, but those constitute a marginal fraction

of our $z = 0$ halo catalog. Thus we also opt to drop the nonlinear velocity dispersion contribution, σ_*, from our modeling.

Finally, taking into account above considerations and for the sake of simplicity, we choose to use a maximally simplified ML estimator, which only includes individual velocity errors in the data weights drawn from a Gaussian distribution independently for each velocity component according to the prescription of Eq. (21).

V. OBSERVER-INDEPENDENT SYSTEMATICS

Here we will present the results of our analysis of the BF and CMN inferred from mock catalogs where the observer location was kept random and unspecified, i.e., it corresponds statistically (after averaging) to a Copernican observer (see more in [50]). By adopting this approach we will be able to study various systematic effects that are, in principle, independent from the location. By doing this we can assess how much the various systematics can affect the measurements in an idealized survey.

A. Bulk flow

We begin by investigating how the sampling rate or number density of tracers used for the measurement affects the resulting BF. In Fig. 3 we show the median bulk flow

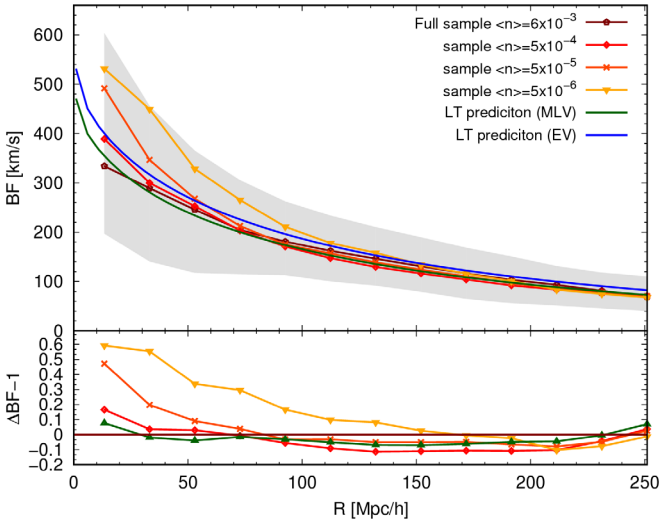

FIG. 3. Comparison of bulk flows estimated from tracer samples with different number densities. Upper panel.—The bulk flow amplitude estimated from simulations (lines with symbols) set together with two linear theory predictions: most likely value (green line) and expected value (blue line). The shaded region marks the interval between 16th and 84th percentiles around the median value for the full sample (pentagons). Diamonds, crosses and triangles correspond to less dense samples of 5×10^{-4}, 5×10^{-5} and 5×10^{-6} (h^{-3} Mpc^3) respectively. Bottom panel.—Relative difference of various tracer samples taken with respect to the full sample result.

measured for the full sample which is characterized by $\langle n \rangle = 6 \times 10^{-3} h^3$ Mpc^{-3}, and for three catalogs with lower number density of tracers, namely $\langle n \rangle = 5 \times 10^{-4}$, 5×10^{-5}, and $5 \times 10^{-6} h^3$ Mpc^{-3}, respectively. We also plot two LT predictions for the MLV and EV. The lower panel of Fig. 3 illustrates the relative differences for the various samples, taken always with respect to the fiducial full one, which includes all the central halos. For the scales $\gtrsim 100 h^{-1}$ Mpc all the samples agree with the fiducial one down to 10%. However, at smaller scales we can notice a clear departure of the BF in the lower number density samples from the fiducial case. The scale at which such deviations start to be noticeable, as well as the magnitude of the effect itself, depend on the number density of objects in the sample. The most diluted sample of $\langle n \rangle = 5 \times 10^{-6} h^3$ Mpc^{-3} is at $100 h^{-1}$ Mpc characterized by median BF amplitude already higher by 15% than for the full one, and this grows dramatically to $+40\% \sim +60\%$ at $R < 50 h^{-1}$ Mpc. At those scales the nonlinear matter distribution leads to strong biasing of mass-weighted estimators based on discrete tracers, thus the observed discrepancy with the volume-weighted LT prediction is not surprising. This discrepancy gets less dramatic the larger the number density we consider. For a sample of $\langle n \rangle = 5 \times 10^{-5} h^3$ Mpc^{-3}, the scale at which the measured BF departs significantly from the fiducial result shrinks to $\sim 50 h^{-1}$ Mpc, but the magnitude still can attain quite remarkable $+50\%$ difference at the smallest scales we consider (i.e., $10 h^{-1}$ Mpc). The subsample of 1 order of magnitude larger number density also deviates from the fiducial case, but only at very small scales $\lesssim 25 h^{-1}$ Mpc, and the relative difference reaches $+20\%$ only for the smallest considered radius.

There is no physical reason for sparser samples to be characterized by larger bulk flow magnitudes. In particular, we expect that all samples trace the same large-scale regions of a simulated universe. The increase of the amplitude we observe is a purely statistical effect, and very likely a manifestation of the mass-weighting character of the estimator (12). Since the BF distribution is not Gaussian, for sparser samples the shot noise enlarges the width of the BF distribution. This effect combined with an overweighted contribution of the outliers results in the observed artificial increase of the measured BF amplitude. Still, despite the fact that all the differences between the samples are contained within the 16th and 84th percentile variation from the median of the fiducial one, they are of a systematic nature and if ignored could be a source of a significant BF bias, especially at small scales, where in real astronomical surveys the target selection is rather nonuniform. We will discuss the implications of these systematic effects in the discussion Sec. IX.

Separately, we note that the LT MLV is a reasonably good prediction for the true BF at nearly all scales probed. This indicates that choosing suitable integral limits for the

LT predictors (as discussed earlier) allows to properly account for the missing large-scale power.

We now consider the effects induced on our measured BF by applying various weighting schemes. The galaxy weighting prescriptions from Sec. IV are meant to roughly mimic various systematic effects present in real data. Again, we will be gauging the measured bulk flow amplitude with respect to our full sample, which constitutes an idealized fiducial case with the best sampling rates and no systematics present. For each effect we consider, we apply the specific weighting and data transformation separately from all the other effects, every time taking the fiducial full sample as a starting point. The situation as presented in our Fig. 4 looks quite the opposite to what was shown in the previous plot 3. Here, we observe that the systematic effects (if present) start to matter at large scales and grow in magnitude with scale. The effect related to the observational error modeling as in the ML method is quite easy to understand, as the error on the velocity grows linearly with scale. This taken together with the Malmquist bias [103,104] produces a systematic overestimation of the measured BF in relation to the full sample [44]. The scale dependence of the velocity error makes it actually quite easy to model: for the scales of $R \lesssim 120h^{-1}$ Mpc, this weighting overestimates the BF by less than 10%. At larger scales $120 \lesssim R/(h^{-1}\ \mathrm{Mpc}) \lesssim 220$, it saturates the 10% departure that is rather flat, as no clear scale dependence can be seen. At even larger scales the effect grows up to 20%–25% reaching the maximal expected effect related to the scatter of the intrinsic galaxy relation we use of $\sigma_v = 0.25$.

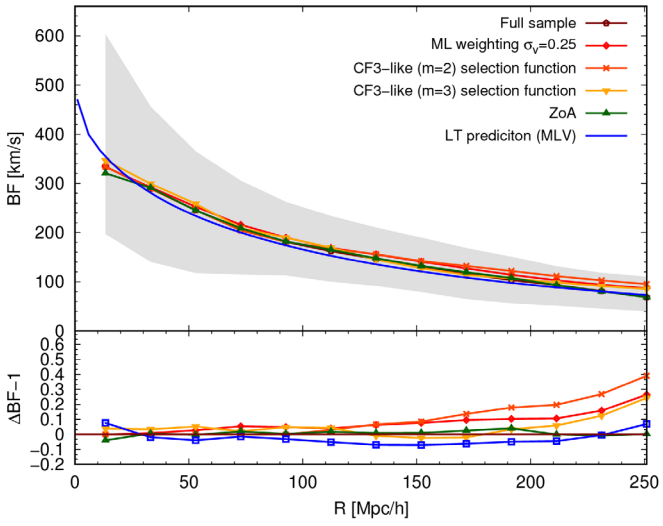

FIG. 4. Comparison of bulk flow amplitudes measured from mock catalogs characterized by different observational effects considered each separately. The shaded region marks the distance between 16-th and 84-th percentiles around the full sample median (pentagons). The comparison is made with velocity error weighting like in the maximum likelihood method (diamonds), CF3-like radial selection with $m = 2$ (crosses) and $m = 3$ (down triangles) and Zone of Avoidance geometry (up triangles). For the reference the linear theory prediction is also shown (blue continuous line). The bottom panel shows the relative differences taken with respect to the full sample values.

The situation is significantly more complicated for the case of a radial selection function that is characteristic of a COSMICFLOWS-3-like data set. Here, there is a clear trend that grows systematically with scale, and is related to the effective depth of the sample. At scales that are above this characteristic depth, r_w, which for our case is $80h^{-1}$ Mpc, the BF is grossly overestimated. At $R = 150h^{-1}$ Mpc such a radial selection already biases the measurement by $+10\%$ and this quickly grows to values of $+40\%$ and larger for $R \gtrsim 200$–$250h^{-1}$ Mpc.

When we look at the geometrical selection effect of the ZoA as modeled by us, our results confirm the findings of other authors. Namely we find it to have a negligible effect on the measurements, as expected for the case of a symmetric data masking. We re-emphasize however that this is valid under the assumption of no significant nearby structures present in the ZoA, an effect that we do not investigate in the current paper.

B. Cosmic Mach number

In this paper we analyze also the cosmic Mach number (CMN or $\mathcal{M}$, interchangeably), which, as mentioned earlier, is the ratio of the BF and peculiar velocity dispersion. The $\mathcal{D}$ in a given sphere centered on the observer is not directly observable, however there have been some indirect methods proposed to measure the CMN [52,55,57]. Thus, we will not present and separately discuss the above-mentioned sampling and weighting effects for the VD alone, but rather for the sake of brevity we show the combined effects on the actual CMN itself. This is presented in Fig. 5. Again as the reference line we take the fiducial measurement from the full sample.

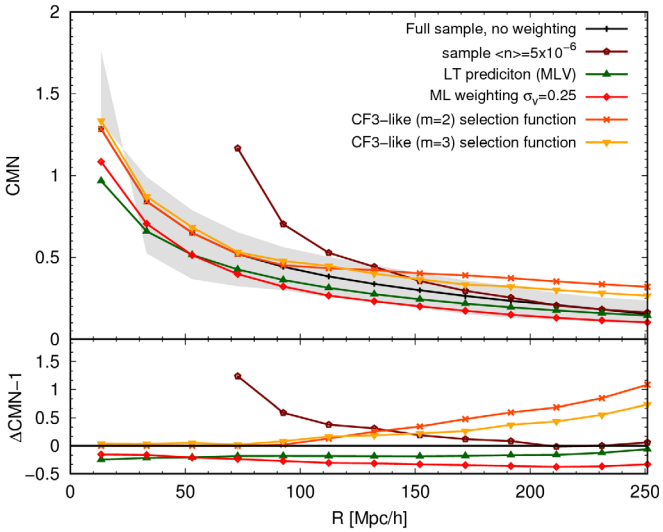

FIG. 5. Analogous to Figs. 3 and 4 but for the cosmic Mach number, defined as in Eq. (19).

The first observation to make is that the magnitude of all visible systematic effects is significantly larger for the $\mathcal{M}$ than it was for the BF. This is not surprising and stems from two facts. First, the VD is a much more nonlinear quantity than the BF, as the former strongly depends on short-wavelength modes; and second, the CMN is a ratio of two quantities and thus the overall effect of systematic biases and uncertainties is boosted. Moving towards more specific cases, we note that a sparse sample of $\langle n\rangle = 5\times 10^{-6}h^3$ Mpc^{-3} leads to a strongly biased $\mathcal{M}$ estimate for scales $\lesssim 150h^{-1}$ Mpc. Here, the deviation from the fiducial case increases with diminishing scale, from +25% up to more than +100% bias in a sphere of radius $75h^{-1}$ Mpc. We were not able to probe the CMN for that sample on smaller scales, since the shot noise from small number counts in such a sparse sample dominates there. Even for $R < 100h^{-1}$ Mpc we should be careful with interpreting our result, as the mean number of objects in such a volume is then $\langle N\rangle < 10$.

For the case of modeled velocity errors, the estimator clearly provides too low a $\mathcal{M}$. We have checked that this is a combination of two effects. Namely, as previously shown, the velocity errors lead to overestimation of the BF, which enters the denominator in the CMN formula. At the same time the velocity errors naturally lead to underestimation of the local $\mathcal{D}$. These two combined effects make such a CMN estimator, mimicking real data properties, significantly biased at all probed scales.

The situation becomes even more severe for the case of CF3-like radial selection functions. Here, both examined selections offer highly biased $\mathcal{M}$ estimators for all scales larger than the characteristic survey depth r_w, and the systematic effects quickly become catastrophically large. At $R \lesssim r_w$ the estimated CMN is very close to the fiducial case; this is not a surprise, as here the radial selection is still complete (i.e., is equal to unity). Finally, it is also important to note that for the case of the $\mathcal{M}$, the LT predictor does not offer a reliable estimator. This is clearly shown in Fig. 5: LT significantly underestimates the CMN for all the considered scales. As we have already assessed that the LT offers a reasonably good prediction for the BF, we then conclude that it must be the VD which is underestimated. Indeed, this is clearly the case, as was already hinted at by the results shown in Fig. 2. In addition, we need to remember that we use mass-weighted estimators, which reconstruct a momentum rather than a pure velocity field. In addition, the averaging procedure in which $\mathcal{M}$ is obtained also plays a role here. Reference [54] has showed that here the following inequality holds:

$$\left(\frac{\langle\mathcal{B}^2\rangle}{\langle\mathcal{D}^2\rangle}\right)^{1/2} < \left\langle\frac{|\mathcal{B}|}{\mathcal{D}|}\right\rangle < \left\langle\frac{\mathcal{B}^2}{\mathcal{D}^2}\right\rangle^{1/2}. \tag{26}$$

We use the intermediate relation for our CMN definition, which is closer to the physical meaning of this statistics. The above relation indicates that even in the case of unbiased volume-weighted fields our estimator will be giving higher values than the LT prediction based on the left-hand-side relation.

VI. BIASES FOR LOCAL GROUP OBSERVERS

In this section we will test and quantify potential biases that arise in the measurements of the lowest moments of the peculiar velocity field if one neglects the fact that the related observations available to us come from a specific location in the Universe. In other words, we will compare ensemble medians of the low-order moments of the galaxy velocity field measured by unspecified observers, whom we will call *random observers* (**RNDO**), and different observers placed at specific locations which fulfill various criteria we consider to be related to the position of a local group (LG) analog observer. The work of Ref. [50] has shown that such *LG observers* (**LGO**) can exhibit highly biased local velocity correlation measurements.

To stay consistent with this previous study we will consider exactly the same selection criteria used to define a set of LG-analog observers. For clarity we give here all the essential information, referring the reader looking for more specific details or discussion to the original work. The LG is a gravitationally bound system of a dozen major galaxies with the Milky Way (MW) and its neighboring M31 as the major gravitational players. The region of 5 Mpc distance from the LG barycenter is characterized by moderate density (see e.g., [101,105–108]) and a quiet flow [109–112]. Located at a distance of $\sim 12h^{-1}$ Mpc is the Virgo cluster, whose gravitational effects extend to tens of Mpcs around us, as evident from the corresponding infall flow pattern of galaxies [113–118]. The presence of such a large nonlinear mass aggregation can and does have substantial impact on peculiar velocity field of the local galaxies.

To find locations of prospective LG-like observers we use the following criteria:

1. The observer is located in a MW-like host halo of mass $7\times 10^{11} < M_{200}/(h^{-1}\ M_\odot) < 2\times 10^{12}$ [119–122].
2. The bulk velocity (of smoothed DM velocity field) within a sphere of $R = 3.125h^{-1}$ Mpc centered on the observer is $V = 622 \pm 150$ km s^{-1} [123].
3. The mean density contrast within the same sphere is in the range of $-0.2 \le \delta \le 3$ [124–126].
4. A Virgo-like cluster of mass $M = (1.2\pm 0.6)\times 10^{15}h^{-1}\ M_\odot$ is present at a distance $D = 12\pm 4h^{-1}$ Mpc from the observer [114,127].

To examine the role of individual criteria we also study results for sets of observers selected without imposing all the above constraints. The sets of observers we consider are:

[**LGO0**] a set of the most constrained 2294 observers, each satisfying all the selection criteria 1 through 4;

[**LGO1**] consists of 5051 candidate observers without the velocity constraint 2, but satisfying the remaining criteria 1, 3 and 4;
[**LGO2**] includes 4978 candidates without the density contrast condition 3, but with 1, 2 and 4;
[**LGO3**] of 4840 candidates with the conditions 2 and 3 relaxed simultaneously, i.e., meeting 1 and 4;
[**LGO4**] a set of 6245 observers without imposing the constraint on the host halo mass 1, but with all the other criteria 2–4 fulfilled;
[**LGO5**] contains 288424 candidate observers satisfying the conditions 1–3 but not the proximity to a Virgo-like cluster 4;
[**RNDO**] is a list of observers with randomly selected positions in the simulation box. This set is used as a benchmark for comparison.

Since the number of prospective candidates in each set is large, to keep the sampling noise at the same level and also to speed up the calculations we will only consider 125 observers from each set. Since positions of observers are not independent of each other, we subsample the candidates by placing a $5 \times 5 \times 5$ grid in the simulation box and keeping only one unique observer location within each grid cell. All the results shown in this section were obtained by taking the median of the distribution for all the 125 observers in each set.

A. Bulk flow

Figure 6 illustrates the systematic effects on the median BF as measured by various observers. As the reference we take the Copernican observer of an unspecified location. In other words, we expect that the **RNDO** observers measure the expected cosmic mean values. Indeed, the results shown in the previous section agree with this assumption, as the BF measured for the random observers agrees well with the LT prediction (Fig. 3). The shaded region in Fig. 6 again illustrates the width of the distribution of measured bulk flows between the 16th and the 84th percentiles.

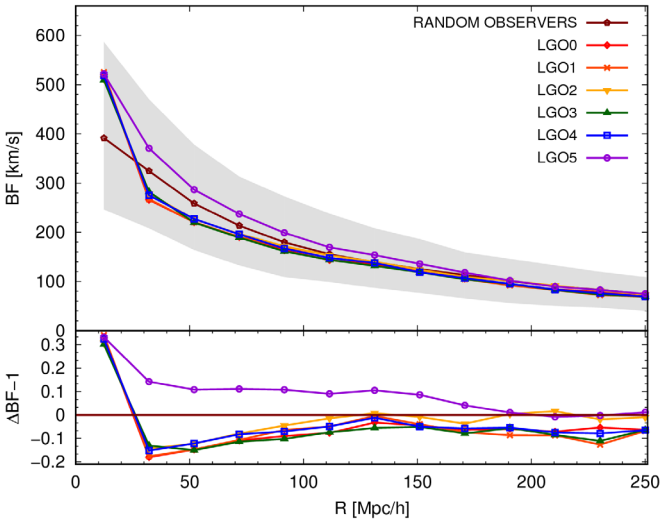

FIG. 6. Comparison of the median bulk flow measured by a random observer against those inferred for various Local-Group-like observers (see text for details). *Upper panel.* The amplitude of the median bulk flow measured for an ensemble of observers of a given class. *Bottom panel.* Relative differences taken with respect to the fiducial random observer case.

A quick look at the results for different nonrandom observers already allows us to find a striking feature: there is only one criterion really discriminatory for the results. Namely, what matters here is the proximity of a Virgo-like cluster to the observer. All **LGO** analogues who fulfill the latter requirement measure a BF that is systematically smaller than the cosmic mean for $R \lesssim 125h^{-1}$ Mpc. This effect is around $\sim 10\%$ at $\sim 100h^{-1}$ Mpc and grows to even 20% for scales smaller than $50h^{-1}$ Mpc. Additionally, we see that the LG position requirements considered without the proximity of a Virgo-like analogue also have an effect on the measured BF. Interestingly, this seems to work in the opposite direction than the other joint criteria, and an LG-analogue but no-Virgo observer would measure actually a systematically larger BF than a random one. This means that the effect of the Virgo-like object proximity is actually stronger than shown by our LG analogues. We have used a small set of observers with just the Virgo criterion to check that this is indeed the case.

We propose the following interpretation of these findings. The criterion that an observer should be located nearby a massive structure of a Virgo-like mass induces a constraint on the local density (hence also velocity) field when compared to a fully random observer. Such a constraint naturally lowers the scatter among observers [128,129], thus also the BF magnitude. However, one should also bear in mind that the fact that we operate on mass-weighted fields will also matter here and will probably emphasize the role of a Virgo-like mass concentration.

B. Velocity dispersion and cosmic Mach number

We now turn to the importance of observer location for the VD and $\mathcal{M}$ statistics. In Fig. 7 we plot the comparison of median velocity dispersions obtained for the different observers we consider. Here, we notice that the effects imposed by a Virgo-like proximity are contained to somewhat smaller ($\lesssim 90h^{-1}$ Mpc) scales than in the BF case. All our LG analogues with a nearby cluster measure much higher $\mathcal{D}$ (up to 50%) at small scales. This clearly indicates that the effect is purely driven by the presence of a massive nonlinear structure of the cluster. Interestingly however, all the measurements converge to the random value at $R \sim 110h^{-1}$ Mpc.

The effects of the observer location for the CMN statistics are illustrated in Fig. 8. Not surprisingly, it is clear that the overall **LGO** effect is driven mostly by the presence or absence of a nearby Virgo-analogue cluster. This amounts to **LGO** $\mathcal{M}$ bias of the order of $\sim 40\%$ at $R \lesssim 50h^{-1}$ Mpc, which reduces to $\sim 10\%$ at $100h^{-1}$ Mpc. Thus, in the case of CMN one is concerned with an even

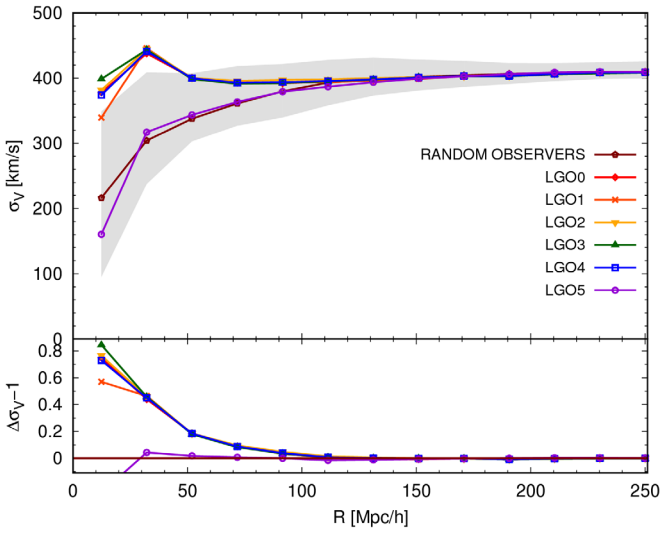

FIG. 7. Comparison between the median velocity dispersion measured by a random observer against those for specific local group observers, analogous to Fig. 6.

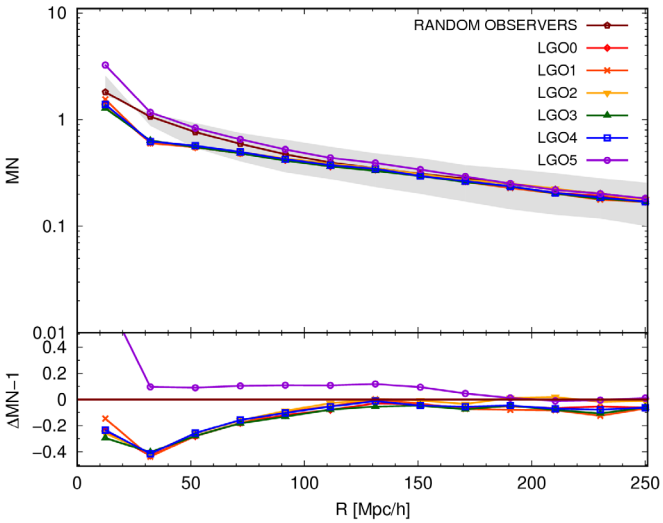

FIG. 8. Comparison between the median cosmic Mach number measured by a random observer against those for specific local group observers, analogous to Fig. 6.

stronger observer bias than in the BF case. This should be remembered and accounted for before any cosmological analysis of this statistics is performed.

VII. GRAVITY AND GROWTH RATE

In the previous sections we have observed that various systematics can significantly change the bulk flow amplitude on a wide range of scales. This fact has fundamental consequences for all applications that hope to use the BF and related statistics such as $\mathcal{M}$ to search for non-GR signature. As an illustration, here we will compare a velocity signal from a modified gravity model against the various observational effects present in the GR case.

For our *guinea pig* MG model we choose the normal branch of Dvali-Gabadadze-Poratti (henceforth nDGP) model [130–132], which implements the nonlinear fifth-force screening (the Vainshtein mechanism) [133] and can be characterized at large scales by a nearly constant (i.e., scale-independent) enhancement of the growth rate of structures (see also [134]). Specifically we choose to take the value of the so-called crossing-over scale to be $r_c H_0 = 1$. This value represents the scale at which gravity becomes five-dimensional in this model. The smaller this scale, the stronger deviations from GR dynamics (due to the fifth force) can be expected. Our choice of r_c gives moderate modifications to GR that are characterized by a linear growth rate (the logarithmic derivative of linear density growing mode) $f_{\rm nDGP} \approx 1.15 f_{\rm GR}$ [135–137]. Except for the modified dynamics induced by the scalar field present in the nDGP model, our MG simulation shares exactly the same setup and parameters as the fiducial GR case. For the sake of speeding-up the numerical computations we have employed the truncated DGP method described in detail in [138]. The speed-up is obtained at the expense of the resolution of the scalar-field spatial fluctuations, solving of which was truncated beyond the fourth mesh refinement level. This sets the resolution of the scalar force at $\sim 60h^{-1}$ kpc, which is still considerably smaller than the smallest halos we consider. As we use the same initial conditions for both GR and nDGP, the large-scale cosmic variance effects should be of the same magnitude in both runs (see also [139]), and the observed discrepancies should reflect the differences in the underlying gravitational dynamics.

Figure 9 compares the BF measured by two Copernican observers, one in GR and one in the nDGP model (marked as MG), versus the amplitudes expected in the GR case with different systematic effects. For the sake of brevity, we choose to compare with only the strongest systematics elucidated in the previous section. In particular, we show the **LGO**0 and **LGO**5 signals, as well as **RNDO** observers with sparse sampling of $\langle n \rangle = 5 \times 10^{-6} h^3$ Mpc^{-3}. For $R \lesssim 200h^{-1}$ Mpc, the MG bulk flow is enhanced by $\sim$10%, as one can expect from the LT prediction of Eq. (16). This potentially observable effect can be easily obscured by various systematics that have larger magnitudes on the same scales. Specifically, we see that realistic modeling of the local group analogue observers, which includes the effects of the Virgo cluster proximity, gives opposite sign to the MG enhancement. Thus, in the worst case scenario, we could have a conspiracy, where a BF signal for a **LGO**0 observer in an MG universe would look like a BF expected for a **RNDO** observer in the GR universe. On the other hand, the signal expected for a **LGO** observer modeled without a Virgo-like cluster presence can mimic the scale dependence and amplitude of a **RNDO** MG signal. For a very sparse sample, these two observations would be dwarfed by a systematic effect that on small

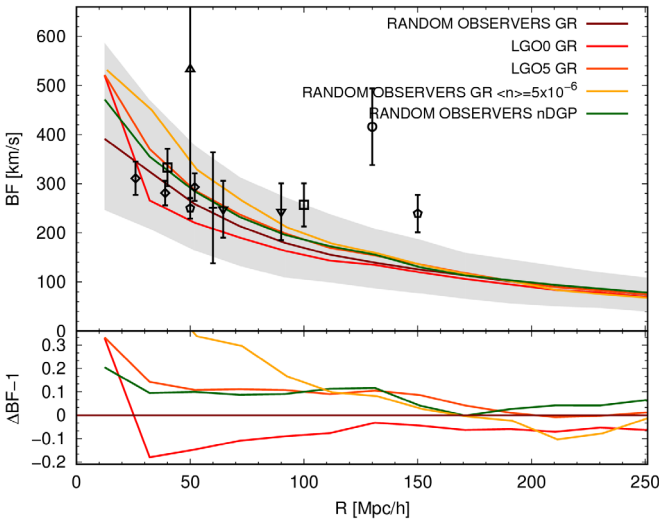

FIG. 9. The median bulk flow as measured by random observers in GR and nDGP gravity model compared with GR-observer measurements affected by various systematics. The data points illustrate some recent $\mathcal{B}(R)$ measurements from the literature: dash—Branchini *et al.* [30]; pentagrams—Hoffman *et al.* [22]; diamonds—Hong *et al.* [38]; down triangles—Scrimgeour *et al.* [42]; up triangle—Lavaux *et al.* [34]; squares—Nusser and Davis [15]; and circle—Feldman *et al.* [140].

scales ($R \lesssim 100h^{-1}$ Mpc) can be by a factor of a few times larger than what we can expect for a reasonably mild MG model enhancement.

The main merit of our work here is to systematically study potential biases of low-order velocity measurements, but it is illustrative to compare the scales and amplitudes of the effects we report with some $\mathcal{B}(R)$ measurements reported in the literature. We have selected arbitrarily seven such measurements and marked them in Fig. 9. We show results from Branchini *et al.* [30], Hoffman *et al.* [22], Hong *et al.* [38], Scrimgeour *et al.* [42], Lavaux *et al.* [34], Nusser and Davis [15] and Feldman *et al.* [140]. The methods and data sets used in these references vary significantly, so this collection is a fair representation of approaches and data used currently in peculiar velocity studies. Except for Refs. [22,140], all the results are consistent within 16th and 84th percentiles with median $\mathcal{B}$ of random and **LGO** observers and even with the MG model. If we took the size of the error bars reported by those authors at their face values, some of our results (such as the MG model) would be marginally inconsistent with that data. However, we clearly see that the variance added by the systematic effects will boost the reported error bars significantly.

The results shown here can have potentially profound repercussions, as it would seem that the lower-order velocity statistics are plagued by potentially overwhelming systematic effects that can completely obscure even relatively strong (∼10%) deviations from the GR case. We shall discuss the implication of these findings in the next section.

VIII. SUMMARY

In this paper our main aim was to methodically check various possible systematic effects that could affect the measured values of the bulk flow, peculiar velocity dispersion, and cosmic Mach number. Peculiar velocities of galaxies strongly depend on the underlying cosmic parameters, such as the logarithmic growth rate (f) and the nonrelativistic matter energy density (Ω_m). Velocity data are prone to large uncertainties stemming from the intrinsic scatter of various empirical galaxy scaling relations used to measure redshift-independent distances, and consequently, infer peculiar velocities. The latter are additionally affected by such issues as non-Gaussian errors and nonlinear (i.e., virial) contributions. Many methods have been proposed and implemented to deal with these issues. However, once the velocity data had been corrected for intrinsic errors and Malmquist biases, it was commonly assumed that the relevant statistics could be directly related to the underlying cosmology using theoretical modeling (such as linear perturbation theory). This assumed advantage was one of the main arguments for using the galaxy velocities as alternative cosmological probes. In our analysis we have revisited this assumption, and our results indicate that there are many systematic effects that need to be accurately modeled and accounted for, in order to infer cosmological parameters from low-order velocity statistics in an unbiased manner.

Below we summarize and comment on all our important findings and their implications.

Perturbation theory estimators:

1. The results encapsulated in Fig. 2 show that strong modulations of the density power spectrum amplitude lead to only mild variations in BF and VD. More precisely, we have found that the changes in both statistics are roughly proportional to changes in f and σ_8.
2. Using the nonlinear velocity divergence power spectrum instead of the nonlinear density $P(k)$ has a strong effect on the predicted $\mathcal{D}$, and therefore also on the $\mathcal{M}$. This is because the magnitudes of the effects induced in the nonlinear regime are opposite in those two spectra. Namely, at small scales the nonlinear $P_{\theta\theta}(k)$ takes smaller values than the linear theory prediction, while the nonlinear $P(k)$ has actually a boosted amplitude with respect to the linear theory. At small scales in the nonlinear regime the motions of galaxies lose the character of a potential flow. This reflects significant growth of vorticity and velocity dispersion due to shell crossing [84,90,92,141]. For that reason it is important to take into account and model properly these nonlinear effects, in order to get a more realistic perturbation theory prediction for the CMN.

Sampling rate effects:

1. At small scales (i.e., $\lesssim 50h^{-1}$ Mpc) we found a significant effect on BF magnitude from undersampling. For increasingly diluted samples the inferred BF is biased towards higher values when compared to our fiducial full sample, and the effect is larger, the smaller the sample density. This is a statistical effect induced by the non-Gaussian distribution of BF magnitudes and increased shot-noise contribution due to sparse sampling. For the sparsest sample with $\langle n \rangle \geq 10^{-6} h^3$ Mpc^{-3}, the bias could attain 50% or more. This indicates that one should carefully account for this effect when low-order velocity statistics are measured from very sparse samples like supernovae [29,32,33,41].
2. The down-sampling of the data we have performed is essentially equivalent to weighting the data by the local value of the density correlation function, since galaxies are biased tracers and form preferentially in higher-density regions. Such regions are characterized by higher values of local bulk flows.
3. Our results show that the MLV estimator from linear perturbation theory is in good agreement with the N-body data for a random-location BF observer.

Selection effects:

1. Weighting halo velocities according to velocity errors induced by distance errors (like in the ML method) leads to overestimation of the BF. This effect grows with distance from the observer, but it saturates to a maximum value that is close to the considered typical scatter of the distance indicator error σ_v.
2. For a radial selection function of a CF3-like survey form, it is evident that the limited depth of the catalog is reflected in the measured BF. The BF is formally an integral over a sphere, but for a realistic survey of discrete galaxies, it becomes a sum over concentric spherical shells of growing radius. The radial selection function is effectively down-weighting the outer shells, and thus the BF value derived from inferior spheres is spuriously propagated to larger scales. This is a strong effect, which indicates that BF measurements from scales comparable or larger than the characteristic depth of a given catalog should be interpreted with care.
3. A symmetric sky-map angular incompleteness with an opening angle of ~ 10 deg—such as the zone of avoidance—has a negligible effect on the inferred BF.
4. All systematic effects related to galaxy selection are much more pronounced in the CMN statistic. In particular, both sparse sampling and velocity errors induce a significant $\mathcal{M}$ bias for scales $\lesssim 150h^{-1}$ Mpc.
5. A radial selection function of the CF3-like form induces a catastrophically large CMN overprediction for scales larger than the given survey characteristic depth.

Observer location effects:

1. For all our low-order statistics the most important **LGO**-analogue criterion is the proximity of a Virgo-like cluster.
2. Local group-analogue observers measure systematically smaller BF amplitudes than the cosmic mean (i.e., a random observer) on scales up to $R \simeq 125h^{-1}$ Mpc. This systematic attains $\sim 10\%$ at $\sim 10h^{-1}$ Mpc and grows to $\sim 20\%$ for $R \lesssim 50h^{-1}$ Mpc.
3. A no-Virgo observer (i.e., **LGO**5) at the same time exhibits an opposite bias, inferring a BF that is larger by $\approx 10\%$ on similar scales than $\mathcal{B}$ measured by the **RNDO** observers.
4. For the VD the LG-observer bias is contained to somewhat smaller scales $R \lesssim 90h^{-1}$ Mpc, but its magnitude reaches a quite dramatic value of up to 50%. This effect is purely driven by the proximity of a Virgo analogue, as a no-Virgo observer measures VD values compatible with **RNDO** observers. This indicates that an infall region around a massive cluster is significantly heating up the local velocity field.
5. The effects observed for BF and VD combine into a biased $\mathcal{M}$ for **LGO** observers, which manifests itself as $\sim 40\%$ underevaluation at $< 50h^{-1}$ Mpc, and still takes $\sim 10\%$ too small a value at $R \sim 100h^{-1}$ Mpc.

Growth rate and gravity:

1. The effect of an increased growth rate f observed in a representative MG model is degenerate with the specific bias induced by a **LGO** observer, and the Virgo-like cluster proximity in particular.
2. Similarly, a non-Virgo **LGO**-like BF signal appears very similar to the MG signal for a **RNDO** observer.
3. Finally, we notice that the BF magnitude increase observed in GR for a sparse sample of $\langle n \rangle = 5 \times 10^{-6} h^3$ Mpc^{-3} is stronger than the non-GR effect of our MG model.

IX. DISCUSSION

The above summary of all our important findings regarding various systematic effects that impact low-order moments of the galaxy velocity field, underlines a number of crucial observations. The linear theory predictions (for MLV) obtained using Eqs. (14)–(18) render quite accurate values of BF for a "cosmic mean" (i.e., *Copernican*) observer in the case of high-density clean data. Thus, they can be used as a first order prediction for the case when all systematic effects can be ignored, or when there are no computer simulations to be compared with. However, we caution that whenever one wants to compare such LT predictions to the real data, one needs to remember that the local galaxy velocity field is biased with respect to the LT prediction at small scales and for sparse or radially incomplete samples.

Currently, the velocity data is sparse and noisy; however, in the near future they will increase significantly in volume. There is also hope for better modeling and understanding of galaxy intrinsic scaling relations, which can lead to further suppression of individual velocity errors. The surveys such as TAIPAN [47] or WALLABY [48] will lead to an increase both in richness as well as depth of galaxy peculiar velocity catalogs. In addition, the possibility to obtain transverse velocities from surveys like GAIA [142] or LSST [143] could result in additional largely unbiased velocity measurements for the nearby galaxies (for a dedicated discussion see [144]). In this new era of velocity data, the linear theory predictions for $\mathcal{B}$ and related statistics will be too inaccurate to be used for model testing and data analysis, except for the large scales (i.e., ≥ 100–$150h^{-1}$ Mpc), where the precision and data abundance will continue to be poor.

The various observer-independent systematic effects surfacing strongly in our analysis suggest that the bulk flow amplitude and related measurements at small distances should be carefully reanalyzed and compared with predictions based on galaxy-mock catalogs. The higher BF values reported by Refs. [22,24,30,35,38,39] might be a signature of biases induced by sparse sampling and radial selection.

The importance of proper modeling of such nonlinear effects is of paramount importance for the cosmic Mach number predictions. This was already emphasized by Ref. [58] for the case of improving the LT predictions by using the nonlinear matter density power spectrum rather than the linear one. Here, our analysis adds further that sparse sampling induces a very strong effect on the VD and thus on the resulting CMN. In addition, other systematics such as radial selection and velocity errors affect $\mathcal{M}$ to a much stronger extent than BF. This suggests in particular that one should aim at using the richest possible galaxy samples when considering CMN measurements.

The proximity of a Virgo-like cluster to a local-group-like observer is equally significant and needs to be considered as an additional important contribution to the local bulk flow. If this effect is not properly accounted for in the BF analysis, it will result in an additional non-Gaussian systematic for the BF measured on scales $R \lesssim 100h^{-1}$ Mpc.

Finally, the combination of all the aforementioned systematic effects, if not accounted for carefully, can lead to strong degeneracies of the cosmological signals encoded in galaxy velocities and in their low-order moments. We have clearly demonstrated that the signal of a non-GR cosmological model, such as the nDGP modified gravity we considered, that employs a moderately strong modification to the cosmic growth rate of structures, can be easily absorbed by the nontrivial systematics effects we studied. In light of this evidence, analyses such as for example Ref. [145], where the BF deviations induced by modified gravity were studied, should be definitely revisited.

All this is a source of potentially major concern, as the cosmic velocity data offers, at least in principle, a model-independent way to constrain growth rate and gravity on cosmic scales [22,37,46,60,146]. Other authors have also shown that current and future data show promise to become competitive cosmological probes [13,14]. In principle, this can still be achieved. However, the results presented here clearly indicate that all the various systematic effects need to be carefully addressed and accounted for, before any high-accuracy cosmological analysis can be performed. This is especially important that in the near future the amount of peculiar velocity data is expected to significantly increase, and therefore systematics will likely dominate over statistical errors in relevant studies. In this context, using dedicated computer simulations employing constrained local density (and velocity) realizations (such as [147–155]) look very promising.

ACKNOWLEDGMENTS

The authors are very grateful to Baojiu Li for inspiring discussions and for providing the ECOSMOG code that was used to run the simulations in this paper. We would also like to thank the anonymous referee whose comments and suggestions helped improve the scientific merit and quality of the manuscript. Enzo Branchini, Martin Feix and Adi Nusser are also acknowledged for stimulating discussions and for careful reading of the manuscript. W. A. H. is supported by an Individual Fellowship of the Marie Skłodowska-Curie Actions and therefore acknowledges that this project has received funding from the European Union's Horizon 2020 research and innovation program under the Marie Skłodowska-Curie Grant Agreement No. 748525. M. B. is supported by the Netherlands Organization for Scientific Research, NWO, through Grant No. 614.001.451, and by the Polish National Science Center under Contract No. UMO-2012/07/D/ST9/02785. This project has also benefited from numerical computations performed at the Interdisciplinary Centre for Mathematical and Computational Modelling (ICM), University of Warsaw, under Grants No. GA67-17 and No. GA65-30. This work used the COSMA Data Centric system at Durham University, operated by the Institute for Computational Cosmology on behalf of the STFC DiRAC HPC Facility [156]. This equipment was funded by a BIS National E-infrastructure Capital Grant No. ST/K00042X/1, DiRAC Operations Grant No. ST/K003267/1 and Durham University. DiRAC is part of the National E-Infrastructure.

APPENDIX: FINITE VOLUME EFFECTS

Here we will investigate how and on what scales the limited simulation volume affects our measurements. As mentioned in the main text, the cosmic velocity field is characterized by a large correlation length. This means that the convergence of velocity moments is slower than in the case of the density field. For that reason we can expect that scales which are normally considered as converged will be

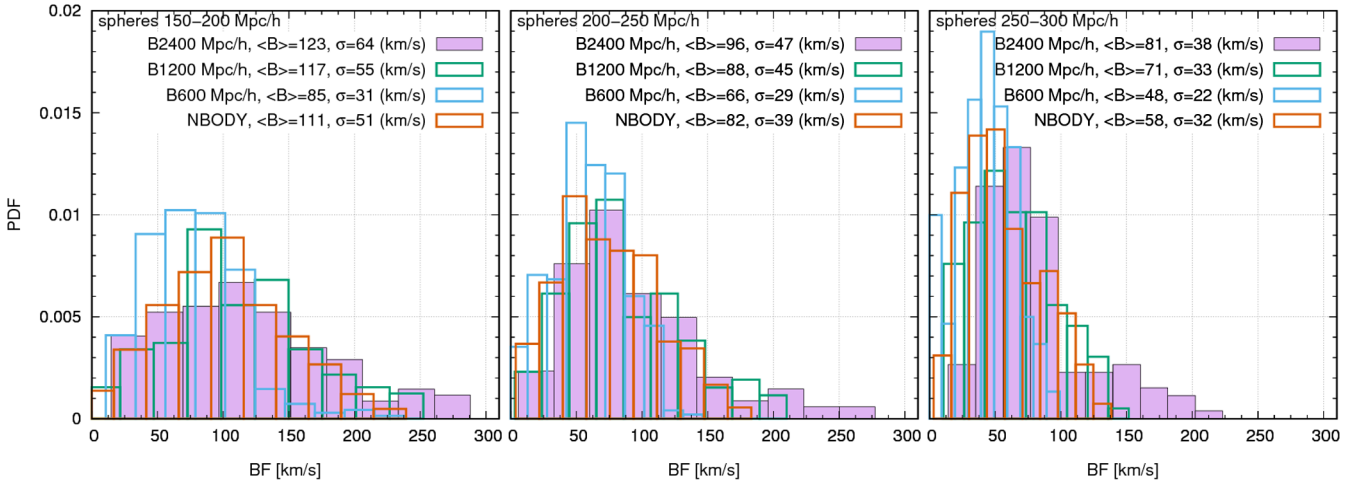

FIG. 10. The distribution of $\mathcal{B}$ magnitudes for three different spheres for our COLA runs. The left-hand side panel considers spheres of radii from 150–200h^{-1} Mpc, the middle panel is for a range of 200–250h^{-1} Mpc, while the right-hand side plot illustrates the results for 250–300h^{-1} Mpc. In each panel the filled boxes are for the fiducial 2400h^{-1} Mpc box, the open green boxes mark the 1200h^{-1} Mpc run and the open blue boxes the 600h^{-1} Mpc one. The open red boxes mark the results from the full N-body run. In each label a median value $\langle\mathcal{B}\rangle$ for a given distribution is given together with σ, which marks a corresponding distribution spread between the 16th and 84th percentiles.

still affected by missing large-scale modes in our simulations. To assess this we have conducted a series of auxiliary approximated simulations varying the box size. For this we employ the *comoving Lagrangian accelerator* (COLA) method [157,158]. The parallel implementation of the COLA algorithm (called PI-COLA, see [159]) allows to run large simulations at a reduced computational cost, with the trade-off of limited spatial and temporal resolution. We are however here interested in the effect of the missing large-scale modes, thus the scales which we will study, namely 100–300h^{-1} Mpc, are large enough to be fully resolved by the PI-COLA method. In particular, we have used the publicly available optimized branch of the COLA family, the MG-COLA, introduced by Ref. [160].

We ran three simulations, all containing 1600^3 volume elements, with three boxes: 600,1200 and 2400h^{-1} Mpc on a side. The simulations are set to use the same cosmology as our main N-body runs used in this work. We process the simulation outputs at $z = 0$ in the same manner as our full N-body simulations. We use the final ROCKSTAR halo catalogs as our input data. The COLA method is known to bias weakly the resulting halo velocities. However, this bias is small (up to ∼5% for our case) and concerns mostly the small-scale halo velocity field (see more in Ref. [161]). Since our primary concern here is to study the effects of missing large-scale power, we are confident that halo catalogs obtained via the simplified COLA method are suitable for our purpose.

In Fig. 10 we show probability distribution functions of $\mathcal{B}$ magnitudes for our COLA runs computed and binned for spheres of three radii: 150–200h^{-1} Mpc in the left-hand panel, 200–250h^{-1} Mpc for the middle one, and 250–300h^{-1} Mpc for the right-hand panel. The PDF for the fiducial run of 2400h^{-1} Mpc box is illustrated by filled purple boxes, while two consecutively smaller simulations are depicted by open green (1200h^{-1} Mpc) and blue (600h^{-1} Mpc) boxes. For comparison we also plot the relevant PDFs for the full N-body simulation used in the paper. The immediate impression is that all the results for the smallest box are significantly biased with respect to the fiducial case. Both the median of the distribution ($\langle\mathcal{B}\rangle$), as well as its spread (σ) [162] are visibly smaller for all three radii. The corresponding relative differences taken with respect to the fiducial case here (i.e., the largest box) are ∼30% (31%) and ∼50% (38%) for the median and spread of the PDF at 150–200h^{-1} Mpc (200–250h^{-1} Mpc) and ∼40% and ∼42% at 250–300h^{-1} Mpc. This is a clear manifestation of the lacking large-scale power in the simulation box. Thus we can, not surprisingly, conclude that the halo velocity field is not converged at those scales in the 600h^{-1} Mpc box. The situation for the medium box 1200h^{-1} Mpc is much better though. Here, the medians are off by only ∼6% (∼8%) at 150–200h^{-1} Mpc (200–250h^{-1} Mpc), while the corresponding distribution widths are smaller by ∼14% (∼5%). However, at the largest radius of 250–300h^{-1} Mpc the biases grow to ∼12% for the median and ∼13% for the width. Our full N-body simulations use a 1000h^{-1} Mpc box, and it is reassuring to find biases of their adequate $\mathcal{B}$ distributions to lie between COLA 1200 and 600h^{-1} Mpc boxes. At $200 \leq R(h^{-1}\,\mathrm{Mpc})^{-1} \leq 250$ the median is biased by more than 14% already. This shows that all the results in this paper for spheres larger than $R \gtrsim 200h^{-1}$ Mpc are noticeably affected by missing large-scale power.

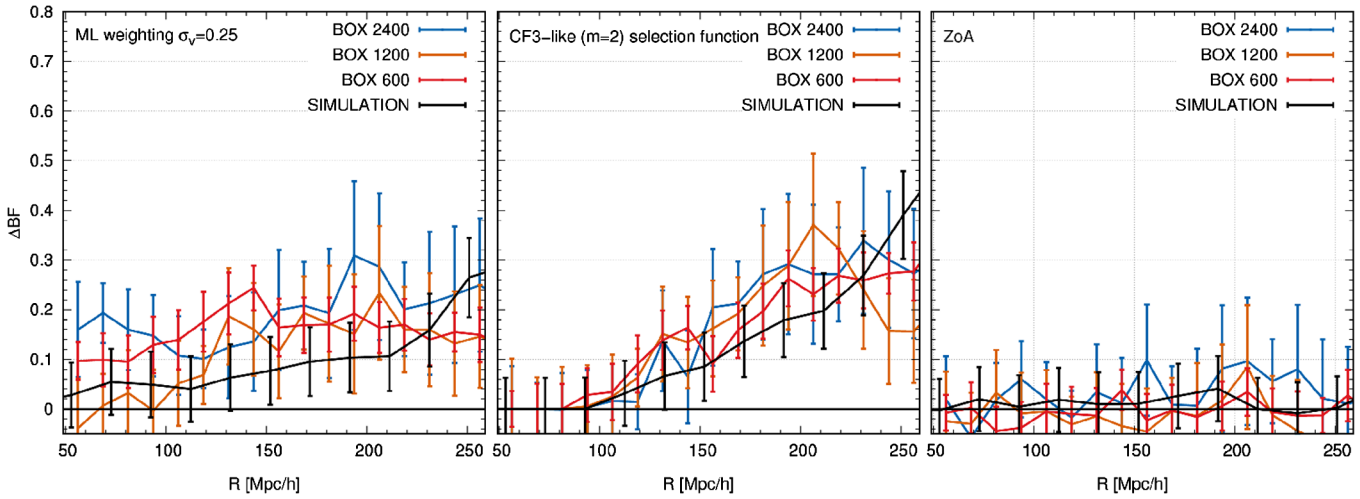

FIG. 11. The relative differences ΔBF taken between the fiducial full sample $\mathcal{B}(R)$ and for various data weighting effects. Each panel compares the results for three COLA boxes and our N-body simulation, while the particular modeled effect varies from panel to panel. The left-hand side considers ML individual velocity error weighting, the middle plot shows a CF3-like radial selection with $m = 2$, and the right-hand side panel presents the effect of ZoA modeling. In each panel the error bars mark the error on the relative ratio computed using the bootstrapped errors on the median $\mathcal{B}$ for 100 random observers.

Obtaining a reliable and accurate absolute bulk flow (and corresponding dispersion) magnitude is of paramount importance when one wants to compare it with astronomical data and use such a comparison for parameter constraints. In this paper however, we are more interested in some specific effects that affect the velocity field statistics in a systematic way. Thus, to study to what scales we can trust our results we present Fig. 11. Here, we compare size of relative differences (taken always with respect to the fiducial unweighted sample) for three systematic effects: ML velocity error weights (left panel), CF-3-like (with $m = 2$) radial selection function (middle panel) and the effect of the zone of avoidance (right panel). Reassuringly, we denote that in all three cases the scale dependence as well as $\Delta\mathcal{B}$ magnitude are very similar (within the sampling error) for the three COLA runs and our full N-body. The largest differences appear for the individual velocity error weights. Here, the N-body results for $R \gtrsim 200h^{-1}$ Mpc are consistently 1σ below the $2400h^{-1}$ Mpc COLA line. This indicates that for the case of this systematic effect and at those scales our results render only the lower bound, and a more realistic modeling will probably foster larger effects.

Finally, we can report that the $\mathcal{B}(R)$ distributions (both from COLA and N-body) at all probed scales are deviating significantly from a Gaussian, with typical skewness (S_3) and kurtosis (S_4) taking values $|S_3|, |S_4| \sim 1$.

[1] G. Hinshaw *et al.*, Astrophys. J. Suppl. Ser. **208**, 19 (2013).
[2] P. A. R. Ade *et al.* (Planck Collaboration), Astron. Astrophys. **594**, A13 (2016).
[3] J. Yang, M. S. Turner, D. N. Schramm, G. Steigman, and K. A. Olive, Astrophys. J. **281**, 493 (1984).
[4] T. P. Walker, G. Steigman, H.-S. Kang, D. M. Schramm, and K. A. Olive, Astrophys. J. **376**, 51 (1991).
[5] W. J. Percival *et al.*, Mon. Not. R. Astron. Soc. **327**, 1297 (2001).
[6] M. Tegmark *et al.*, Astrophys. J. **606**, 702 (2004).
[7] F. Beutler *et al.*, Mon. Not. R. Astron. Soc. **466**, 2242 (2017).
[8] A. G. Riess, A. V. Filippenko, P. Challis, A. Clocchiatti, A. Diercks, P. M. Garnavich, R. L. Gilliland, C. J. Hogan, S. Jha, R. P. Kirshner, B. Leibundgut, M. M. Phillips, D. Reiss, B. P. Schmidt, R. A. Schommer, R. C. Smith, J. Spyromilio, C. Stubbs, N. B. Suntzeff, and J. Tonry, Astron. J. **116**, 1009 (1998).
[9] S. Perlmutter *et al.*, Astrophys. J. **517**, 565 (1999).
[10] W. J. Percival *et al.*, Mon. Not. R. Astron. Soc. **401**, 2148 (2010).
[11] D. H. Weinberg, M. J. Mortonson, D. J. Eisenstein, C. Hirata, A. G. Riess, and E. Rozo, Phys. Rep. **530**, 87 (2013).
[12] M. A. Strauss and J. A. Willick, Phys. Rep. **261**, 271 (1995).
[13] J. Koda, C. Blake, T. Davis, C. Magoulas, C. M. Springob, M. Scrimgeour, A. Johnson, G. B. Poole, and L. Staveley-Smith, Mon. Not. R. Astron. Soc. **445**, 4267 (2014).

[14] C. Howlett, L. Staveley-Smith, and C. Blake, Mon. Not. R. Astron. Soc. **464**, 2517 (2017).
[15] A. Nusser and M. Davis, Astrophys. J. **736**, 93 (2011).
[16] M. J. Hudson and S. J. Turnbull, Astrophys. J. Lett. **751**, L30 (2012).
[17] T. R. Lauer and M. Postman, Astrophys. J. **425**, 418 (1994).
[18] R. Giovanelli, M. P. Haynes, G. Wegner, L. N. da Costa, W. Freudling, and J. J. Salzer, Astrophys. J. Lett. **464**, L99 (1996).
[19] D. A. Dale, R. Giovanelli, M. P. Haynes, L. E. Campusano, E. Hardy, and S. Borgani, Astrophys. J. Lett. **510**, L11 (1999).
[20] M. J. Hudson, R. J. Smith, J. R. Lucey, D. J. Schlegel, and R. L. Davies, Astrophys. J. Lett. **512**, L79 (1999).
[21] R. Watkins, H. A. Feldman, and M. J. Hudson, Mon. Not. R. Astron. Soc. **392**, 743 (2009).
[22] Y. Hoffman, H. M. Courtois, and R. B. Tully, Mon. Not. R. Astron. Soc. **449**, 4494 (2015).
[23] R. Watkins and H. A. Feldman, Mon. Not. R. Astron. Soc. **447**, 132 (2015).
[24] A. Kashlinsky, F. Atrio-Barandela, D. Kocevski, and H. Ebeling, Astrophys. J. Lett. **686**, L49 (2008).
[25] S. J. Osborne, D. S. Y. Mak, S. E. Church, and E. Pierpaoli, Astrophys. J. **737**, 98 (2011).
[26] P. A. R. Ade *et al.* (Planck Collaboration), Astron. Astrophys. **561**, A97 (2014).
[27] J. Colin, R. Mohayaee, S. Sarkar, and A. Shafieloo, Mon. Not. R. Astron. Soc. **414**, 264 (2011).
[28] A. Nusser, E. Branchini, and M. Davis, Astrophys. J. **735**, 77 (2011).
[29] A. Weyant, M. Wood-Vasey, L. Wasserman, and P. Freeman, Astrophys. J. **732**, 65 (2011).
[30] E. Branchini, M. Davis, and A. Nusser, Mon. Not. R. Astron. Soc. **424**, 472 (2012).
[31] K. Mody and A. Hajian, Astrophys. J. **758**, 4 (2012).
[32] S. J. Turnbull, M. J. Hudson, H. A. Feldman, M. Hicken, R. P. Kirshner, and R. Watkins, Mon. Not. R. Astron. Soc. **420**, 447 (2012).
[33] U. Feindt *et al.*, Astron. Astrophys. **560**, A90 (2013).
[34] G. Lavaux, N. Afshordi, and M. J. Hudson, Mon. Not. R. Astron. Soc. **430**, 1617 (2013).
[35] Y.-Z. Ma and D. Scott, Mon. Not. R. Astron. Soc. **428**, 2017 (2013).
[36] B. Rathaus, E. D. Kovetz, and N. Itzhaki, Mon. Not. R. Astron. Soc. **431**, 3678 (2013).
[37] M. Feix, A. Nusser, and E. Branchini, J. Cosmol. Astropart. Phys. 09 (2014) 019.
[38] T. Hong, C. M. Springob, L. Staveley-Smith, M. I. Scrimgeour, K. L. Masters, L. M. Macri, B. S. Koribalski, D. H. Jones, and T. H. Jarrett, Mon. Not. R. Astron. Soc. **445**, 402 (2014).
[39] Y.-Z. Ma and J. Pan, Mon. Not. R. Astron. Soc. **437**, 1996 (2014).
[40] S. Appleby, A. Shafieloo, and A. Johnson, Astrophys. J. **801**, 76 (2015).
[41] D. Huterer, D. L. Shafer, and F. Schmidt, J. Cosmol. Astropart. Phys. 12 (2015) 033.
[42] M. I. Scrimgeour, T. M. Davis, C. Blake, L. Staveley-Smith, C. Magoulas, C. M. Springob, F. Beutler, M. Colless, A. Johnson, D. H. Jones, J. Koda, J. R. Lucey, Y.-Z. Ma, J. Mould, and G. B. Poole, Mon. Not. R. Astron. Soc. **455**, 386 (2016).
[43] C. M. Springob, T. Hong, L. Staveley-Smith, K. L. Masters, L. M. Macri, B. S. Koribalski, D. H. Jones, T. H. Jarrett, C. Magoulas, and P. Erdoğdu, Mon. Not. R. Astron. Soc. **456**, 1886 (2016).
[44] A. Nusser, Astrophys. J. **795**, 3 (2014).
[45] P. Andersen, T. M. Davis, and C. Howlett, Mon. Not. R. Astron. Soc. **463**, 4083 (2016).
[46] A. Nusser, Mon. Not. R. Astron. Soc. **455**, 178 (2016).
[47] E. da Cunha *et al.*, Pub. Astron. Soc. Aust. **34**, e047 (2017).
[48] A. R. Duffy, M. J. Meyer, L. Staveley-Smith, M. Bernyk, D. J. Croton, B. S. Koribalski, D. Gerstmann, and S. Westerlund, Mon. Not. R. Astron. Soc. **426**, 3385 (2012).
[49] R. B. Tully, H. M. Courtois, and J. G. Sorce, Astrophys. J. **152**, 50 (2016).
[50] W. A. Hellwing, A. Nusser, M. Feix, and M. Bilicki, Mon. Not. R. Astron. Soc. **467**, 2787 (2017).
[51] M. Li, J. Pan, L. Gao, Y. Jing, X. Yang, X. Chi, L. Feng, X. Kang, W. Lin, G. Shan, L. Wang, D. Zhao, and P. Zhang, Astrophys. J. **761**, 151 (2012).
[52] J. P. Ostriker and Y. Suto, Astrophys. J. **348**, 378 (1990).
[53] Y.-Z. Ma, J. P. Ostriker, and G.-B. Zhao, J. Cosmol. Astropart. Phys. 06 (2012) 026.
[54] Y. Suto, R. Cen, and J. P. Ostriker, Astrophys. J. **395**, 1 (1992).
[55] M. A. Strauss, R. Cen, and J. P. Ostriker, Astrophys. J. **408**, 389 (1993).
[56] K. Nagamine, J. P. Ostriker, and R. Cen, Astrophys. J. **553**, 513 (2001).
[57] F. Atrio-Barandela, A. Kashlinsky, and J. P. Mücket, Astrophys. J. Lett. **601**, L111 (2004).
[58] S. Agarwal and H. A. Feldman, Mon. Not. R. Astron. Soc. **432**, 307 (2013).
[59] B. Li, W. A. Hellwing, K. Koyama, G.-B. Zhao, E. Jennings, and C. M. Baugh, Mon. Not. R. Astron. Soc. **428**, 743 (2013).
[60] W. A. Hellwing, A. Barreira, C. S. Frenk, B. Li, and S. Cole, Phys. Rev. Lett. **112**, 221102 (2014).
[61] M. F. Ivarsen, P. Bull, C. Llinares, and D. Mota, Astron. Astrophys. **595**, A40 (2016).
[62] G. Tormen, L. Moscardini, F. Lucchin, and S. Matarrese, Astrophys. J. **411**, 16 (1993).
[63] B. Li, G.-B. Zhao, R. Teyssier, and K. Koyama, J. Cosmol. Astropart. Phys. 01 (2012) 051.
[64] P. A. R. Ade *et al.* (Planck Collaboration), Astron. Astrophys. **571**, A16 (2014).
[65] W. A. Hellwing, M. Schaller, C. S. Frenk, T. Theuns, J. Schaye, R. G. Bower, and R. A. Crain, Mon. Not. R. Astron. Soc. **461**, L11 (2016).
[66] R. Teyssier, Astron. Astrophys. **385**, 337 (2002).
[67] G. Dvali, G. Gabadadze, and M. Porrati, Phys. Lett. B **485**, 208 (2000).
[68] F. Schmidt, Phys. Rev. D **80**, 043001 (2009).
[69] J.-N. Ye, H. Guo, Z. Zheng, and I. Zehavi, Astrophys. J. **841**, 45 (2017).
[70] P. S. Behroozi, R. H. Wechsler, and H.-Y. Wu, Astrophys. J. **762**, 109 (2013).

[71] J. P. Huchra, L. M. Macri, K. L. Masters, T. H. Jarrett, P. Berlind, M. Calkins, A. C. Crook, R. Cutri, P. Erdoğdu, E. Falco, T. George, C. M. Hutcheson, O. Lahav, J. Mader, J. D. Mink, N. Martimbeau, S. Schneider, M. Skrutskie, S. Tokarz, and M. Westover, Astrophys. J. Suppl. Ser. **199**, 26 (2012).
[72] M. Bilicki, T. H. Jarrett, J. A. Peacock, M. E. Cluver, and L. Steward, Astrophys. J. Suppl. Ser. **210**, 9 (2014).
[73] B. Reid *et al.*, Mon. Not. R. Astron. Soc. **455**, 1553 (2016).
[74] A. Aghamousa *et al.* (DESI Collaboration), arXiv: 1611.00036.
[75] I. Pâris *et al.*, arXiv:1712.05029.
[76] J. Guillochon, J. Parrent, L. Z. Kelley, and R. Margutti, Astrophys. J. **835**, 64 (2017).
[77] C. M. Springob, K. L. Masters, M. P. Haynes, R. Giovanelli, and C. Marinoni, Astrophys. J. Suppl. Ser. **172**, 599 (2007).
[78] C. M. Springob, C. Magoulas, M. Colless, J. Mould, P. Erdoğdu, D. H. Jones, J. R. Lucey, L. Campbell, and C. J. Fluke, Mon. Not. R. Astron. Soc. **445**, 2677 (2014).
[79] P. J. E. Peebles, *The large-scale structure of the universe* (Princeton University Press, Princeton, 1980), p. 435.
[80] O. Lahav, P. B. Lilje, J. R. Primack, and M. J. Rees, Mon. Not. R. Astron. Soc. **251**, 128 (1991).
[81] E. V. Linder, Phys. Rev. D **72**, 043529 (2005).
[82] M. J. Chodorowski and P. Ciecielag, Mon. Not. R. Astron. Soc. **331**, 133 (2002).
[83] P. Ciecielg, M. J. Chodorowski, M. Kiraga, M. A. Strauss, A. Kudlicki, and F. R. Bouchet, Mon. Not. R. Astron. Soc. **339**, 641 (2003).
[84] S. Pueblas and R. Scoccimarro, Phys. Rev. D **80**, 043504 (2009).
[85] N. A. Bahcall, M. Gramann, and R. Cen, Astrophys. J. **436**, 23 (1994).
[86] P. Coles and F. Lucchin, *Cosmology: The Origin and Evolution of Cosmic Structure*, 2nd ed. (Wiley&Sons, Chichester, 2002), p. 512.
[87] R. Watkins and H. A. Feldman, Mon. Not. R. Astron. Soc. **379**, 343 (2007).
[88] A. Lewis, A. Challinor, and A. Lasenby, Astrophys. J. **538**, 473 (2000).
[89] R. E. Smith, J. A. Peacock, A. Jenkins, S. D. M. White, C. S. Frenk, F. R. Pearce, P. A. Thomas, G. Efstathiou, and H. M. P. Couchman, Mon. Not. R. Astron. Soc. **341**, 1311 (2003).
[90] C. Pichon and F. Bernardeau, Astron. Astrophys. **343**, 663 (1999).
[91] N. I. Libeskind, Y. Hoffman, M. Steinmetz, S. Gottlöber, A. Knebe, and S. Hess, Astrophys. J. Lett. **766**, L15 (2013).
[92] N. I. Libeskind, Y. Hoffman, and S. Gottlöber, Mon. Not. R. Astron. Soc. **441**, 1974 (2014).
[93] O. Hahn, T. Abel, and R. Kaehler, Mon. Not. R. Astron. Soc. **434**, 1171 (2013).
[94] O. Hahn, R. E. Angulo, and T. Abel, Mon. Not. R. Astron. Soc. **454**, 3920 (2015).
[95] C. Rampf and U. Frisch, Mon. Not. R. Astron. Soc. **471**, 671 (2017).
[96] R. C. Kraan-Korteweg, P. A. Woudt, V. Cayatte, A. P. Fairall, C. Balkowski, and P. A. Henning, Nature (London) **379**, 519 (1996).
[97] R. C. Kraan-Korteweg, M. E. Cluver, M. Bilicki, T. H. Jarrett, M. Colless, A. Elagali, H. Böhringer, and G. Chon, Mon. Not. R. Astron. Soc. **466**, L29 (2017).
[98] R. C. Kraan-Korteweg and O. Lahav, Astron. Astrophys. Rev. **10**, 211 (2000).
[99] R. B. Tully and J. R. Fisher, Astron. Astrophys. **54**, 661 (1977).
[100] S. Djorgovski and M. Davis, Astrophys. J. **313**, 59 (1987).
[101] H. M. Courtois, D. Pomarède, R. B. Tully, Y. Hoffman, and D. Courtois, Astrophys. J. **146**, 69 (2013).
[102] N. Kaiser, Mon. Not. R. Astron. Soc. **231**, 149 (1988).
[103] D. Lynden-Bell, D. Burstein, R. L. Davies, A. Dressler, and S. M. Faber, in *The Extragalactic Distance Scale*, Astronomical Society of the Pacific Conference Series, Vol. 4, edited by S. van den Bergh and C. J. Pritchet (Astronomical Society of the Pacific, San Francisco, CA, 1988), pp. 307.
[104] D. Lynden-Bell, S. M. Faber, D. Burstein, R. L. Davies, A. Dressler, R. J. Terlevich, and G. Wegner, Astrophys. J. **326**, 19 (1988).
[105] R. B. Tully and J. R. Fisher, *Annales de Geophysique* (Cambridge University Press, Cambridge, UK, 1987).
[106] R. B. Tully and J. R. Fisher, *Catalog of Nearby Galaxies* (Cambridge University Press, Cambridge, UK, 1988), p. 224.
[107] M. J. Hudson, Mon. Not. R. Astron. Soc. **265**, 43 (1993).
[108] R. B. Tully, E. J. Shaya, I. D. Karachentsev, H. M. Courtois, D. D. Kocevski, L. Rizzi, and A. Peel, Astrophys. J. **676**, 184 (2008).
[109] A. Sandage, G. A. Tammann, and E. Hardy, Astrophys. J. **172**, 253 (1972).
[110] D. Schlegel, M. Davis, F. Summers, and J. A. Holtzman, Astrophys. J. **427**, 527 (1994).
[111] I. D. Karachentsev, M. E. Sharina, D. I. Makarov, A. E. Dolphin, E. K. Grebel, D. Geisler, P. Guhathakurta, P. W. Hodge, V. E. Karachentseva, A. Sarajedini, and P. Seitzer, Astron. Astrophys. **389**, 812 (2002).
[112] I. D. Karachentsev, D. I. Makarov, M. E. Sharina, A. E. Dolphin, E. K. Grebel, D. Geisler, P. Guhathakurta, P. W. Hodge, V. E. Karachentseva, A. Sarajedini, and P. Seitzer, Astron. Astrophys. **398**, 479 (2003).
[113] R. B. Tully and E. J. Shaya, Astrophys. J. **281**, 31 (1984).
[114] G. A. Tammann and A. Sandage, Astrophys. J. **294**, 81 (1985).
[115] N. Y. Lu, E. E. Salpeter, and G. L. Hoffman, Astrophys. J. **426**, 473 (1994).
[116] D. Gudehus, Astron. Astrophys. **302**, 21 (1995).
[117] I. D. Karachentsev, R. B. Tully, P.-F. Wu, E. J. Shaya, and A. E. Dolphin, Astrophys. J. **782**, 4 (2014).
[118] N. I. Libeskind, Y. Hoffman, R. B. Tully, H. M. Courtois, D. Pomarède, S. Gottlöber, and M. Steinmetz, Mon. Not. R. Astron. Soc. **452**, 1052 (2015).
[119] M. T. Busha, R. H. Wechsler, P. S. Behroozi, B. F. Gerke, A. A. Klypin, and J. R. Primack, Astrophys. J. **743**, 117 (2011).

[120] S. Phelps, A. Nusser, and V. Desjacques, Astrophys. J. **775**, 102 (2013).
[121] M. Cautun, C. S. Frenk, R. van de Weygaert, W. A. Hellwing, and B. J. T. Jones, Mon. Not. R. Astron. Soc. **445**, 2049 (2014).
[122] Q. Guo, A. P. Cooper, C. Frenk, J. Helly, and W. A. Hellwing, Mon. Not. R. Astron. Soc. **454**, 550 (2015).
[123] A. Kogut, C. Lineweaver, G. F. Smoot, C. L. Bennett, A. Banday, N. W. Boggess, E. S. Cheng, G. de Amici, D. J. Fixsen, G. Hinshaw, P. D. Jackson, M. Janssen, P. Keegstra, K. Loewenstein, P. Lubin, J. C. Mather, L. Tenorio, R. Weiss, D. T. Wilkinson, and E. L. Wright, Astrophys. J. **419**, 1 (1993).
[124] I. D. Karachentsev, V. E. Karachentseva, O. V. Melnyk, A. A. Elyiv, and D. I. Makarov, Astrophys. Bulletin **67**, 353 (2012).
[125] A. A. Elyiv, I. D. Karachentsev, V. E. Karachentseva, O. V. Melnyk, and D. I. Makarov, Astrophys. Bulletin **68**, 1 (2013).
[126] R. B. Tully, H. Courtois, Y. Hoffman, and D. Pomarède, Nature (London) **513**, 71 (2014).
[127] S. Mei, J. P. Blakeslee, P. Côté, J. L. Tonry, M. J. West, L. Ferrarese, A. Jordán, E. W. Peng, A. Anthony, and D. Merritt, Astrophys. J. **655**, 144 (2007).
[128] Y. Hoffman and E. Ribak, Astrophys. J. **384**, 448 (1992).
[129] R. van de Weygaert and E. Bertschinger, Mon. Not. R. Astron. Soc. **281**, 84 (1996).
[130] V. Sahni and Y. Shtanov, J. Cosmol. Astropart. Phys. 11 (2003) 014.
[131] A. Lue and G. D. Starkman, Phys. Rev. D **70**, 101501 (2004).
[132] F. Schmidt, Phys. Rev. D **80**, 123003 (2009).
[133] A. Vainshtein, Phys. Lett. B **39**, 393 (1972).
[134] A. Barreira, B. Li, W. A. Hellwing, C. M. Baugh, and S. Pascoli, J. Cosmol. Astropart. Phys. 10 (2013) 027.
[135] K. Koyama and R. Maartens, J. Cosmol. Astropart. Phys. 01 (2006) 016.
[136] B. Li, G.-B. Zhao, and K. Koyama, J. Cosmol. Astropart. Phys. 05 (2013) 023.
[137] B. Bose, K. Koyama, W. A. Hellwing, G.-B. Zhao, and H. A. Winther, Phys. Rev. D **96**, 023519 (2017).
[138] A. Barreira, S. Bose, and B. Li, J. Cosmol. Astropart. Phys. 12 (2015) 059.
[139] W. A. Hellwing, K. Koyama, B. Bose, and G.-B. Zhao, Phys. Rev. D **96**, 023515 (2017).
[140] H. A. Feldman, R. Watkins, and M. J. Hudson, Mon. Not. R. Astron. Soc. **407**, 2328 (2010).
[141] G. Cusin, V. Tansella, and R. Durrer, Phys. Rev. D **95**, 063527 (2017).
[142] J. H. J. de Bruijne, Astrophys. Space Sci. **341**, 31 (2012).
[143] LSS Telescope.
[144] A. Nusser, E. Branchini, and M. Davis, Astrophys. J. **755**, 58 (2012).
[145] J. Seiler and D. Parkinson, Mon. Not. R. Astron. Soc. **462**, 75 (2016).
[146] Y. Hoffman, A. Nusser, H. M. Courtois, and R. B. Tully, Mon. Not. R. Astron. Soc. **461**, 4176 (2016).
[147] S. Gottloeber, Y. Hoffman, and G. Yepes, arXiv: 1005.2687.
[148] H. M. Courtois and R. B. Tully, Astron. Nachr. **333**, 436 (2012).
[149] S. Heß, F.-S. Kitaura, and S. Gottlöber, Mon. Not. R. Astron. Soc. **435**, 2065 (2013).
[150] J. G. Sorce, H. M. Courtois, S. Gottlöber, Y. Hoffman, and R. B. Tully, Mon. Not. R. Astron. Soc. **437**, 3586 (2014).
[151] F. Leclercq, J. Jasche, and B. Wandelt, J. Cosmol. Astropart. Phys. 06 (2015) 015.
[152] T. Sawala, C. S. Frenk, A. Fattahi, J. F. Navarro, R. G. Bower, R. A. Crain, C. Dalla Vecchia, M. Furlong, J. C. Helly, A. Jenkins, K. A. Oman, M. Schaller, J. Schaye, T. Theuns, J. Trayford, and S. D. M. White, Mon. Not. R. Astron. Soc. **457**, 1931 (2016).
[153] J. G. Sorce, S. Gottlöber, G. Yepes, Y. Hoffman, H. M. Courtois, M. Steinmetz, R. B. Tully, D. Pomarède, and E. Carlesi, Mon. Not. R. Astron. Soc. **455**, 2078 (2016).
[154] F. Leclercq, J. Jasche, G. Lavaux, B. Wandelt, and W. Percival, J. Cosmol. Astropart. Phys. 06 (2017) 049.
[155] H. Desmond, P. G. Ferreira, G. Lavaux, and J. Jasche, Mon. Not. R. Astron. Soc. **474**, 3152 (2018).
[156] https://dirac.ac.uk.
[157] S. Tassev, M. Zaldarriaga, and D. J. Eisenstein, J. Cosmol. Astropart. Phys. 06 (2013) 036.
[158] G. Valogiannis and R. Bean, Phys. Rev. D **95**, 103515 (2017).
[159] C. Howlett, M. Manera, and W. J. Percival, Astron. Comput. **12**, 109 (2015).
[160] H. A. Winther, K. Koyama, M. Manera, B. S. Wright, and G.-B. Zhao, J. Cosmol. Astropart. Phys. 08 (2017) 006.
[161] E. Munari, P. Monaco, J. Koda, F.-S. Kitaura, E. Sefusatti, and S. Borgani, J. Cosmol. Astropart. Phys. 07 (2017) 050.
[162] For our purpose here, for a measure of the distribution spread (i.e., σ) we use the half width between the 16th and 84th percentiles.